AR-004-159

DEPARTMENT OF DEFENCE

DEFENCE SCIENCE AND TECHNOLOGY ORGANISATION

ELECTRONICS RESEARCH LABORATORY

TECHNICAL REPORT

ERL-0333-TR

INFRARED DETECTOR RESEARCH
METAL FILM BOLOMETER DETECTORS
PART 3 - PREPARATION AND PERFORMANCE

K.C. Liddiard, J. Hlava and P.D. Girdler

S U M M A R Y

This report describes the preparation and performance of metal film bolometer infrared detectors using a versatile fabrication technology for both single-element detectors and focal plane arrays. Detectors are prepared on conventional semiconductor-grade silicon substrates and extensive use is made of state-of-the-art micro-circuit manufacture techniques. A detectivity of $\sim 2 \times 10^8$ cm.$Hz^{\frac{1}{2}}$.W^{-1} and speed of response of ≤ 1 ms can be achieved, for detector element sizes as small as 50 μm.

POSTAL ADDRESS: Director, Electronics Research Laboratory,
Box 2151, GPO, Adelaide, South Australia, 5001.

TABLE OF CONTENTS

		Page
1.	INTRODUCTION	1
2.	DETECTOR PREPARATION	1
	2.1 Detector materials	2
	2.2 ERL first generation process	2
	2.2.1 Description of the process	2
	2.2.2 Deposition masks	4
	2.2.3 Limitations of the first generation process	4
	2.3 Second generation process	5
	2.3.1 Description of the process	5
	2.3.2 Detector annealing	7
	2.3.3 Detector film adhesion	7
	2.3.4 Comments on pellicle fabrication	7
3.	DETECTOR PACKAGING	8
	3.1 Technical requirements	8
	3.2 Detector package types	9
	3.2.1 SED packages	9
	3.2.2 Platform package	9
	3.2.3 ERL custom package	10
	3.2.4 DIL ceramic package	10
	3.3 Sealing materials	11
	3.3.1 Low melting point solders	11
	3.3.2 Glass sealants	12
	3.3.3 Polymer resins	12
	3.4 Infrared windows	12
	3.4.1 Window materials	12
	3.4.2 AR coatings	12
	3.4.3 Window seals	13
	3.5 Substrate bonding and lead attachment	13
	3.6 Final package seals	14
	3.6.1 Dimple sealing technique	14
	3.6.2 RF and radiant heating techniques	14
	3.6.3 Rim weld seals	15
	3.7 Preferred package sealing technique	15
4.	DETECTOR RESPONSIVITY	15
	4.1 Analysis of responsivity	15

Page

4.1.1 Low frequency responsivity 16
4.1.2 Dependence of responsivity on detector parameters 17

4.2 Measurement of responsivity 17

4.2.1 Measurement of radiant responsivity 18
4.2.2 Electrothermal analogue techniques 19

4.3 Detector element characteristics 20

4.4 Vacuum responsivity 21

4.4.1 First generation detectors 21
4.4.2 Second generation detectors 21

4.5 Dependence of responsivity on gas pressure 22

4.5.1 Dependence on gas type 22
4.5.2 Measured responsivity as a function of pressure 23

4.6 Dependence of responsivity on bias temperature 23

4.7 Thermal conductance 24

4.8 Dependence of responsivity on bias current 25

4.9 Detector responsivity at optimum bias 25

4.9.1 First generation detectors 25
4.9.2 Second generation detectors 26

5. SPEED OF RESPONSE 26

5.1 Measurement of speed of response 26

5.2 Experimental results 27

5.3 Thermal capacitance 27

6. DETECTOR NOISE AND DETECTIVITY 28

6.1 Measurement of detector noise 28

6.2 Excess noise 28

6.2.1 Origin and reduction of excess noise 28

6.3 Piezoresistance noise 29

6.4 Noise limited performance 29

6.5 Detectivity 29

6.5.1 Comments on second generation performance 30

7. BIAS LIMITATIONS AND OPERATIONAL TESTING 31

7.1 Testing of detector resistance 31

Page

7.2 Bias current testing 31

7.3 Bias current limitations 32

7.3.1 Burnout current 32
7.3.2 Long term failure tests 33

7.4 Transients 33

8. SUMMARY AND CONCLUSIONS 34

9. ACKNOWLEDGEMENTS 35

REFERENCES 36

LIST OF TABLES

1. SUMMARY OF PROPERTIES OF DETECTOR MATERIALS 3

2. LOW MELTING POINT SOLDERS 11

3. DETECTOR ELEMENT CHARACTERISTICS 20

4. TYPICAL VACUUM RESPONSIVITY OF FIRST GENERATION DETECTORS 21

5. TYPICAL VACUUM RESPONSIVITY OF SECOND GENERATION DETECTORS 22

6. TYPICAL DC RESPONSIVITY OF FIRST GENERAL DETECTORS AT OPTIMUM BIAS 25

7. TYPICAL DC RESPONSIVITY OF A SECOND GENERATION DETECTOR AT OPTIMUM BIAS 26

8. SPEED OF RESPONSE OF FIRST GENERATION METAL FILM BOLOMETER DETECTORS 27

9. MAXIMUM DETECTIVITY OF MFB DETECTORS 30

10. BURNOUT CURRENT FOR MFB DETECTORS 33

LIST OF FIGURES

1. Cross-sectional schematic of a first generation detector

2. Microphotograph of a first generation detector

3. Vacuum deposition jigs

4. Cross-sectional schematic of a second generation detector

5. Microphotograph of a second generation detector

6. Single element detector mounted on TO5 header

7. Detector array mounted on Tekform platform package base

8. Detector array mounted in ERL package

9. Detector array mounted in a DIL ceramic package

10. Single element detector package with zinc selenide window

11. Tekform platform package with zinc selenide window

12. ERL custom package sealed in vacuo

13. DIL ceramic package sealed by rim weld method

14. Thermal response characteristics of a first generation detector to a thermal step

15. Plot of resistance versus bias power for a first generation detector

16. ac bias record showing detector response at different nitrogen pressures

17. Low frequency responsivity as a function of gas pressure

18. Vacuum responsivity as a function of bias current for a first generation detector

19. Responsivity at atmospheric pressure as a function of bias current for a first generation detector

20. Frequency response curves for a first generation detector

21. Spectrum analyser records of detector noise

22. Detectivity as a function of frequency

1. INTRODUCTION

This report describes the preparation and performance of metal film bolometer (MFB) infrared detectors. The theory of the MFB detector was given in Part 1(ref.1) and Part 2(ref.2) gave an account of materials research associated with detector development.

In the Part 1 report it was predicted that an MFB detector would have a vacuum responsivity of at least 50 $V.W^{-1}$, whilst the responsivity in air at atmospheric pressure would exceed 5 $V.W^{-1}$. These predictions applied to a 189 Ω detector element of thickness ≤ 10 nm, deposited onto a 20 nm thick dielectric pellicle. The estimated speed of response, for a nominal detector size of 0.1 mm x 0.1 mm, was 1.0 ms in vacuo and 200 μs at atmospheric pressure. It was concluded that this performance could be achieved using a high melting point metal as the detector element, and an amorphous inorganic dielectric as the pellicle material.

The ultimate performance of an MFB detector is limited by the Johnson noise of the detector resistance, except at very low frequencies where current noise predominates. The peak detectivity is estimated to be of the order 2×10^8 $cm.Hz^{\frac{1}{2}}.W^{-1}$ in vacuo, decreasing in proportion to the responsivity at high gas pressures. The predicted detectivity approaches within a factor of five of thermal-fluctuation-noise-limited performance.

In this report it is demonstrated that the measured performance of MFB detectors is in good agreement with the theoretical predictions. The overall performance is comparable or superior to commercial thermal detectors.

A description is given of the preparation of both single-element detectors and detector arrays. In the latter case, current development is restricted to 20-element linear arrays; however the technology can be readily extended to two-dimensional focal plane arrays. An important feature is the introduction of silicon substrate technology, which has led to the extensive application of microcircuit device fabrication techniques. In addition to the prospects of low cost manufacture, there is also a considerable 'stretch' potential for further development, including on-chip and hybrid signal processing.

Patent applications related to the work described in this report are given in reference 3.

2. DETECTOR PREPARATION

The thin film bolometer detector developed at Electronics Research Laboratory (ERL) consists of an ultrathin self-absorbing metal film detector element, which is deposited onto an amorphous dielectric pellicle. The infrared sensor, comprising the detector element and pellicle, is supported over a hole or slot formed in a bulky substrate. A description of research on detector materials, and the development of pellicle and substrate technologies, is given in reference 2. This report is concerned with the preparation of operational detectors, and consideration is given only to preferred detector and pellicle materials. Furthermore only silicon substrate technology will be discussed.

Two basic methods of detector preparation are described in this section. The first method, now referred to as the 'first generation process', was wholly developed at ERL, and has been used to produce detector arrays for experimental infrared detection systems. The second method, which employs on-the-plane microcircuit processing, was devised at ERL and is under joint

development with Australian industry. This advanced 'second generation' process will replace the previously established technology, and is expected to become the basic technique for future development of new generations of thin film thermal infrared detectors.

2.1 Detector materials

As stated above, the discussion will be restricted to preferred materials, and relevant data extracted from reference 2 is summarised in Table 1. It will be noted that data for both first and second generation processes are included in the table, distinguished as options 1 and 2. Note also that silicon nitride is an acceptable alternative to aluminium oxide for detector pellicles, and is in fact used in detectors processed by Australian industry.

2.2 ERL first generation process

The preparation of detectors proceeds through three distinct stages, each representing a functionally complete operation. These are:

(a) preparation of detector substrates,

(b) preparation of pellicle films, and mounting of pellicles on individual substrates, and

(c) preparation of detector elements.

An attractive feature of the technology is the ability to 'batch-process' at each of the above stages; ie, the preparation of substrates, or the preparation and mounting of pellicles, can be accomplished separately and the components stored for subsequent use as required. This is a particularly useful concept, since the process is suitable for small laboratories, but can also be readily adapted to larger scale production.

An important characteristic of the first generation process is that both pellicles and detector elements are prepared by vacuum deposition, using precision micromechanical masks to define detector geometry. These operations are essentially 'dry' processes which, although perfectly adequate for many detector designs, have certain limitations which will be described later (Section 2.2.3).

2.2.1 Description of the process

The process commences with anisotropic chemical etching of V-groove slots in the front and rear surfaces of a standard 50.8 mm diameter, 280 mm thick, thermally-oxidised silicon wafer. These (100) surface orientation wafers are polished on the front surface and bright etched on the rear surface, and have a resistivity in the range 1 to 100 Ω.cm. The rear surface slots function as venting holes to avoid pellicle fracture during evacuation.

Interconnect and bonding pad metallisation is applied to the front surface of the wafer using conventional photolithography. The three-component metallisation is comprised of sputter-deposited films of titanium, platinum and gold, similar to that used in beam-lead style devices. At least 25 10 mm x 5 mm array substrates or 200 5 mm x 1.5 mm single element detector substrates are prepared on a single silicon slice, using step-and-repeat photomasks. The processed substrates are separated by means of a diamond microcircuit dicing saw.

TABLE 1. SUMMARY OF PROPERTIES OF DETECTOR MATERIALS

Substrate	
Material	Single crystal silicon, (100) surface orientation
Method of preparation	1. Anisotropic front surface etch to form pellicle aperture, rear surface venting etch 2. Anisotropic rear surface etch to form pellicle aperture, with boron-doped etch stop
Etchant	1. Hydrazine at 115°C 2. EDP at 110°C
Conductor metallisation	1. Sputter-deposited Ti:Pt:Au 2. EB deposited aluminium
Pellicle	
Material	Aluminium oxide
Thickness	25 nm
Density	2.75 $g.cm^{-3}$
Thermal conductivity	0.03 $W(cm.K)^{-1}$
Method of preparation	1. EB deposition, polymer membrane mounting technique(*) 2. EB deposition direct onto substrate
Detector element	
Material	Platinum
Thickness	4 nm
Density	15 $g.cm^{-3}$
Thermal conductivity	0.15 $W(cm.K)^{-1}$
Electrical conductivity	1.3 to 2.0 x 10^{4} $(\Omega.cm)^{-1}$
Temperature coefficient of resistance	1. 0.08%.K^{-1} 2. 0.12%.K^{-1}
Method of preparation	1. EB deposition, micromechanical mask 2. EB deposition, patterned by photolithography
Post deposition annealing	1. Air at 250°C 2. Air at 500°C
Detector contacts	1. 35 to 75 nm thick gold film 2. As for substrate metallisation

Note: Option 1. First generation processing
Option 2. Second generation processing

* Pellicle films are prepared by electron beam deposition of aluminium oxide through precision micromechanical masks onto cellulose nitrate membranes. The pellicle film is pressed onto the substrate with the aid of an accurate locating jig, and the polymer membrane backing is then removed using RF plasma ashing. This renders the pellicle freely-supporting over the slot in the front surface of the substrate.

The platinum detector elements are electron beam deposited through precision micromechanical masks onto the pellicle, followed by the deposition of gold film contacts, which electrically bridge the detector elements to the interconnect metallisation.

Finally, the completed detector is subjected to air annealing at 250°C. Annealing stabilises the electrical resistance of the detector and enhances the temperature coefficient of resistance by a factor of about 2 above that of the as-deposited detector film.

A cross-sectional schematic of a complete detector is shown in figure 1, and a microphotograph of an actual detector is included at figure 2.

The process was developed with extensive support by Advanced Engineering Laboratory (AEL). Silicon wafers were oxidised and diced by Philips Electronic Components and Materials, Hendon, SA, and photomasks were prepared by AWA Microelectronics, Sydney, NSW, using master artwork designed at ERL.

2.2.2 Deposition masks

The precision micromechanical masks employed for the deposition of pellicle films, gold film contacts and detector elements, were manufactured in AEL. The masks consist of 100 µm thick electro-formed nickel, with the desired patterns generated by photolithography using the lift-off technique. A 50 µm deep aperture was incorporated in each mask, which acted as a spacer to avoid direct mechanical contact with the pellicle or (in the case of pellicle deposition) the polymer membrane.

Excellent edge definition was achieved, and the smallest mask dimension reliably produced was 50 µm. The masks were mechanically robust and capable of withstanding routine cleaning schedules.

The masks were inserted in stainless steel deposition jigs provided with spring clamps to lock the substrates in the correct position. Mask patterns included registration markers, and provision was made in the deposition jig design for alignment of masks to corresponding registration markers patterned on detector substrates. Fine adjustment was achieved for detector element and contact depositions by inserting the jigs in a mask aligner, the actual adjustment being carried out under a conventional biocular microscope.

Detector deposition hardware, including detector element and contact deposition jigs, resistance monitor and temperature probes, jig holder and mask aligner, are shown in figure 3. Under this laboratory scale operation, four deposition jigs are used in a single process (two jig locations are occupied by resistance and temperature probes in experimental work, leaving four locations for deposition jigs). Five single element detector substrates or one array substrate are accommodated in each jig. In the case of pellicle deposition, each deposition jig provides for five single element detector pellicles or two array pellicles. As a production process, these numbers could be greatly increased.

2.2.3 Limitations of the first generation process

Whilst the first generation processing technique is relatively efficient compared to methods used for other types of thermal infrared detectors, there are nevertheless certain limitations, which are briefly outlined below:

(a) The pellicle mounting technique is a manual process, and is prone to defects caused by substrate surface contamination (these can be minimised in a clean room environment).

(b) Although the pellicle, when mounted, is mechanically robust, it will not withstand wet processing.

(c) Pellicle adhesion depends on physical bonding to the substrate surface, and the pellicle itself replicates the polymer surface onto which it is initially deposited.

(d) The use of evaporation masks restricts detector geometry to simple rectangular shapes of minimum dimensions of about 50 μm. This in turn limits the range of detector resistance (typically 150 to 500 Ω), and imposes strict control on the deposition process.

(e) Individual substrates must be manually loaded into deposition jigs.

(f) Annealing is limited to a temperature of about 300°C.

It should be noted that a detector element size of 50 μm is small for a thermal infrared detector and typical for a photon detector, and the ability to produce detectors of this size has been an important feature of development at ERL. However, if the detectors could be formed by photolithography, the scope for expanding the technology would significantly increase. The major thrust of the advanced detector research programme has been the development of a wholly planar (photolithographic) process based on microcircuit device technology.

2.3 Second generation process

The second generation process was devised at ERL and is being developed jointly with AWA Microelectronics(AWAM), Sydney, NSW. The main features of the technology(ref.4) are that detector materials are deposited (by any convenient method) on the front surface of a silicon wafer, the detector element and conductor metallisation (contacts, interconnects and bonding pads) are patterned by conventional photolithography, and the pellicle is formed as the final step by back-etching through the rear surface of the silicon substrate.

This process offers the ability to fabricate precise pellicle windows and a variety of detector designs. Other advantages include a higher annealing temperature, utilisation of various deposition and microcircuit processing techniques, the ability to fabricate a number of individual detectors (or detector arrays) on the same silicon slice, and integration with silicon microcircuit devices for signal processing.

At the current stage of development, the process has been demonstrated at ERL and AWAM, and work is being directed towards resolving minor technical problems and optimising the process technology for manufacture in Australian industry.

2.3.1 Description of the process

Detector substrates are (100) surface orientation silicon wafers used for microcircuit manufacture. Standard 50.8 mm (2 inch) wafers are employed for research studies at ERL, whilst 76.2 mm (3 inch) slices are used at AWAM.

The first steps in the process are the generation of thermal oxide

masks, which are used to produce etched registration markers and to selectively boron dope the front surface of the substrate. The boron doping acts as an etch-stop to ensure precise window definition. A thermal oxide mask is also used for the final rear surface etch. Optional mask materials, such as silicon nitride or a suitable metal film, may be used for registration markers and rear surface etching; however thermal oxide masks are used throughout at ERL.

Following boron doping, the remaining thermal oxide is removed and the wafer is re-oxidised. It is then necessary to remove the oxide over the window (non-doped areas), and this is readily achieved by using the photographic reversal of the doping mask. At this stage, it is important to form a small slope in the oxide at the edge of the window, in order to provide a good step coverage for the detector film. For research purposes, it is sufficient to thin the oxide and rely on the undercutting profile beneath a poorly adherent photoresist layer. A more suitable method is to sputter-deposit a silicon dioxide film onto the thermal oxide prior to patterning, thereby attaining controlled undercutting of the photoresist due to the faster etch rate of the sputtered oxide. A proprietory process is employed at AWAM to ensure good step coverage.

A ledge of 200 to 300 nm height is formed at the edge of pellicle windows as the result of oxidation during boron drive-in. This ledge must also be taken into account in the detector design, but thus far has presented no discernible processing problems.

The next step is to deposit the pellicle film onto the front surface of the wafer. Electron-beam-deposited aluminium oxide is used at ERL, whilst excellent results have been achieved at AWAM with CVD-deposited silicon nitride. The deposition conditions must be selected to ensure that the pellicle film is in neutral or slight tensile stress at the completion of the process.

The platinum detector film is then deposited onto the front surface and the detector element pattern is formed photolithographically using plasma etching or the lift-off technique (in the latter case, deposition follows photoresist patterning). Both methods have been demonstrated at ERL, and lift-off is used at AWAM. Sputter etching produces good results, but the pellicle film is also eroded. Preliminary experiments with RF plasma etching have suggested that this technique has excellent potential, but lack of availability of a suitable dedicated reactor has led to current preference for the lift-off method.

Detector deposition is followed by deposition and patterning of contact-interconnect-bonding pad metallisation. Either gold-based or conventional aluminium metallisations are suitable, but the latter is currently preferred at both ERL and AWAM.

In the final process step, pellicle windows are produced by rear surface etching through a thermal oxide mask, using hydrazine or ethylene diamine/pyrocatechol etchants. The etch process produces V-grooves at an angle of 54.7° to the surface plane. The etching slows at the boron-doped regions on the front surface, but continues through to the pellicle film at the non-doped (window) areas. Note that vertical side wall etch profiles have been achieved at ERL with (110) orientation silicon wafers, but for current work the V-groove profile is preferred. Further details are given in reference 2.

The wafer is diced by cracking along separation lines produced during the back etch process. The separation lines are included on the same

photomask used to generate the rear surface thermal oxide etch mask.

Because detector elements are defined by conventional planar photolithography, a variety of shapes and sizes are possible. Both single element and arrays of detectors can be prepared, and by means of step-and-repeat artwork, a number of detectors can be fabricated on the same wafer. Detector elements with sizes of 50 µm up to 1.0 mm, and resistances from 100 to 10 000 Ω have been prepared, with shapes ranging from simple strips to fine zig-zag patterns. The versatility of the process technique also offers the ability to produce special low thermal conductance detector designs.

A cross-sectional schematic of a complete detector is shown in figure 4. Current emphasis is being directed towards a 20-element array design having a zig-zag detector element of effective size 70 µm x 70 µm, some 70 of which are produced on a single 76.2 mm diameter wafer. A microphotograph of an actual detector fabricated at ERL is shown in figure 5.

2.3.2 Detector annealing

Detectors are annealed in air at 400 to 500°C. Annealing is usually carried out following the detector metallisation processing step; however it has been found that detectors will withstand heat treatment up to 500°C after etching and separation.

The resistance of platinum bolometers begins to rise when the annealing temperature approaches 500°C, because of the formation of a volatile oxide film. However, the highest temperature coefficient of resistance was observed for detectors annealed at 500°C, and it was also found that the adhesion of platinum films improves with annealing.

2.3.3 Detector film adhesion

A particular problem associated with the second generation process is the need to achieve strong adhesion of detector film materials to their underlying substrates. This problem arises because of wet processing and cleaning requirements, which are capable of removing weakly adherent films.

Platinum film detector elements do not bond strongly to the preferred pellicle materials, and hence some form of adhesion promotion is necessary. Annealing in air improves adhesion, and at the current state of progress annealed detectors will survive to the back-etch stage, but survival through the final etch is marginal.

AWAM has found that a brief flash of titanium prior to platinum deposition ensures satisfactory adhesion through the entire process. There is evidence that this ultrathin titanium film affects the electrical properties of the detector, notably reducing the temperature coefficient. Research is underway at ERL to resolve this problem, including an investigation of alternative metals such as nickel.

2.3.4 Comments on pellicle fabrication

Hydrazine has been employed at ERL and AWAM for back-etching of silicon, whilst ethylene diamine/pyrocatechol (EDP) has been investigated as an alternative etchant at ERL. Both etchants deteriorate with use - hydrazine should be replaced after 3 to 5 operations because of irregular etching and introduction of wafer contamination, and EDP must be freshly prepared for each batch of wafers due to rapid deterioration

in air.

Hydrazine etching slows on reaching the boron-doped areas at the front surface of the wafer, but since the etch rate of the doped silicon is still appreciable, precise timing is required to avoid complete loss of the etch-stop region. By comparison, EDP etching virtually ceases when the boron concentration exceeds 7×10^{-19} cm^{-3}, and EDP is consequently the preferred etchant for future work. As stated above, EDP etchant must be changed regularly, and the etch process should be carried out in an inert gas atmosphere.

It is known that heavily boron-doped silicon is in high tensile stress, with the result that fine (microscopic) cracks often appear in the etch-stop region surrounding pellicle windows. However, these regions remain mechanically strong, and so far there has been no instances of detector damage (eg fracture) due to mechanical defects of this nature. A proposal by AWAM to employ a suitably doped epitaxial layer as an etch stop merits favourable consideration in future development of the back-etch technique.

A particular problem experienced with hydrazine and EDP etchants is the formation of small pyramids during the etch process. These hillocks originate at defects in the silicon wafer, and can be removed by using a higher hydrazine content or, in the case of EDP, a higher proportion of ethylene diamine. Unfortunately, the choice of etch solution involves a trade between etch rate, hillock formation and degree of anisotropy. A compromise is adopted at ERL(ref.2), to ensure minimum hillock formation and good overall etch characteristics. However, this comprise results in a short etchant life, since the depletion of reactants leads to a rapid increase in hillock density and reduction in etch rate.

3. DETECTOR PACKAGING

The work conducted at ERL on packaging technology for thin film bolometer detectors has been concerned with the development of a low cost microcircuit-style package which can be evacuated or filled to a predetermined pressure with a selected gas. An important consideration is the desire to devise a technology which can be readily established in the Australian microelectronic industry.

Infrared detectors are usually sealed in specially designed packages, and in some instances (notably the evacuated dewar used with cooled photon detectors) the package represents a substantial proportion of the total detector cost. Adaptation of transistor packages for single element detectors or small arrays is well known, evacuation being achieved by means of a pumping tube and tip-off technique. Uncooled thermal detectors operated at atmospheric pressure are now widely sealed in custom microcircuit packages. However the use of a low cost package of conventional design, which can be evacuated and sealed by routine large scale operations, presents a number of unique technical problems.

3.1 Technical requirements

The pressure requirement for an evacuated package is not severe, since it is necessary to maintain a pressure of only 1 Pa (7.5 mtorr) in order to ensure maximum detector responsivity. Nevertheless, there are special problems associated with small volume, low cost packages, in particular:

(a) The package must be free of real leaks, and thus totally effective seals are required.

(b) The package must have a low virtual leak rate (ie, outgassing), because of the small volume and difficulty of installing getters.

(c) A simple and effective method must be devised for sealing infrared-transmitting windows.

(d) A large pin count may be required in the smallest possible package size.

The general approach to these problems has been to develop specialised techniques and materials technology at ERL, and to adapt the technology to conventional packaging methods employed in the microcircuit industry. Thus ERL work is concerned with sealing metallurgy, infrared window design, outgassing properties of materials, etc, whilst effort in industry is directed towards the actual production technique for sealing and testing of detector packages.

3.2 Detector package types

A particular problem experienced with detector package development is the difficulty of procuring suitable packages in the small quantities required for experimental purposes. This has led to the selection of packages based on availability rather than optimum design. These packages are thus used to establish a satisfactory sealing technology, the aim then being to design and procure a dedicated custom package for full scale manufacture, following similar practice widely adopted in the microcircuit industry.

3.2.1 SED packages

Conventional T05 and T039 transistor packages were used exclusively for single element detectors(SED). These packages were particularly suitable for the standard 5 mm x 1.5 mm SED substrates. They differ only in the base dimensions, one (the T039) having a weld rim.

The packages are cheap, readily available and have a good dimensional tolerance (at least within the same production batch). The caps fit neatly, with little distortion and hence minimum gap between cap and base.

Vacuum tight base seals were achieved with a range of low melting point solders (see Section 3.3.1). The commercial caps were modified, by means of a precision punch, to accept a 5 mm diameter x 1 mm thick infrared transmitting window (Section 3.4.1). The aperture in the cap is 3 mm diameter. Successful window seals were made with low melting point solders and low vapour pressure epoxy resins.

A photograph of an SED detector mounted on a T05 header is shown in figure 6.

3.2.2 Platform package

A Tekform No. 20234 20-pin platform package was used for 20 element first generation detectors arrays. This package appeared to be particularly suitable for 10 mm x 5 mm array substrates, the only obvious disadvantage being the need to connect the detector common rail to the package base. However it was found that the rectangular lids were slightly distorted (as-provided, including different batches), and the maximum spacing between lid and base was about 0.1 mm. This meant

that substantial pressure was required during base sealing, leading to more complex vacuum sealing apparatus and the added risk of fracturing the infrared window seal.

A precision punch was again used to modify the commercial lid to accept a 12.5 mm long x 7.5 mm x 1 mm thick infrared transmitting window. The aperture in the lid is 10 mm x 5 mm. Vacuum tight window seals were achieved using low melting point solder alloys (Section 3.4.3).

Because of the difficulty of making a reliable base seal, these packages were used extensively for gas-filled operation at atmospheric pressure. A dimple sealing technique was employed for xenon-filled packages (Section 3.6.1). A polymer resin was used for the base seal. subsequent experience with these xenon-filled packages showed a deterioration in performance consistent with either outgassing within the package or a leakage through the seal.

Some packages were fitted with a copper pumping tube for evaluation of detector performance in vacuo and in partial pressures of various gases.

A photograph of a 10 mm x 5 mm array substrate mounted on a platform package base is shown in figure 7.

3.2.3 ERL custom package

In order to examine the properties of various materials for vacuum packaging applications, a special 24-pin circular package was designed and manufactured at ERL. This package is machined from Macor glass-ceramic bar stock and comprises a 26 mm diameter circular disc, onto which is deposited a thick-film conductor pattern, and a 2 mm thick annulus sealed onto the disc with Vitta glass transfer tape. The top of the annulus is polished, and a sputter-deposited metal coating is applied for window sealing.

The thick film metallisation extends beneath the glass seal to make contact with standard 0.5 mm diameter package pins or side-braze flat pins. The package is designed for installation in a dedicated sealing jig located in a vacuum chamber. The package can be fully outgassed in vacuo, and the final seal is a one-step operation comprising sealing of the circular infrared window to the top face of the annulus. Some packages were fitted with a copper pumping tube for detector evaluation.

A photograph of a 10 mm x 5 mm detector array substrate mounted in an ERL package is shown in figure 8.

3.2.4 DIL ceramic package

The package selected by AWA Microelectronics for evaluation of microcircuit sealing techniques is a Kyocera 24 lead side-braze ceramic package of conventional dual-in-line (DIL) design, fitted with a rim weld sealing ledge around the rectangular recess in the package. The flat lid is 0.25 mm thick, thinned at the periphery to 0.075 mm. The thinned area enables location of the lid over the package recess, and is of the desired thickness for the rim weld operation.

The infrared transmiting window is sealed over an aperture in the centre of the lid. Both the window and aperture dimensions are the same as that used for the Tekform platform package.

A photograph of a 10 mm x 5 mm array substrate mounted in a DIL ceramic package is shown in figure 9.

3.3 Sealing materials

An extensive investigation has been made of various low melting point solder alloys, glass-based sealing materials, and polymer resins. A summary of experimental results is given in the following subsections.

3.3.1 Low melting point solders

The various solders investigated in the project are listed in Table 2.

TABLE 2. LOW MELTING POINT SOLDERS

Composition	Melting temperature (°C)	Form
80 gold 20 tin	280	preform
90 gold 10 tin	490	multilayer preform
96 tin 4 silver	221	wire or preform
100 indium	157	wire or preform
90 indium 10 silver	237	wire
50 indium 50 tin	125	wire

Of the materials listed in Table 2, 80Au20Sn was obtained as a commercial preform, 90Au10Sn preforms were prepared in AEL, and the remaining solders were extruded from ingots and shaped in AEL and ERL. AEL has now developed an electroformed preform capability for indium solders.

Because fluxless seals are required, the sealing temperature is usually substantially higher than the melting (liquidus) temperature, in order to overcome surface oxide and induce solder flow. In addition, the solder must be confined to the bonding area, and the sealing surfaces must be in close mechanical contact. A further problem is experienced when a package requires two seals, eg window and base, since the final seal must not disturb previous seals. This means using either different solders or controlled (differential) package temperatures. Note that temperature gradient considerations will always apply, because the detector and its bonding material (ie the solder or resin used to affix the substrate to the package) must withstand the sealing operation.

Temperature limitations led to rejection of the excellent 80Au20Sn solder in favour of lower temperature solder seals. Initial investigations were dedicated to the development of a 90Au10Sn pressure-diffusion bonding technique. This technique uses a multilayer tin-gold-tin preform prepared by electroforming or vapour deposition. The seal is made under pressure at a temperature of approximately 232°C (melting point of tin). The melting point of the final seal is 490°C.

In general, diffusion bond techniques (whereby controlled seals are made well below the liquidus temperature of the alloy composition) are considered a highly desirable method of package sealing. However further work on this approach was abandoned because of the effort required to achieve full characterisation (time/temperature data), and the difficulty of obtaining adequate surface contact between sealing faces with the available packages.

Vacuum-tight window seals are achieved on a routine basis at ERL using

96Sn4Ag solder alloy. Simple solder seals have also been successfully demonstrated with pure indium, 90In10Ag, and 50In50Sn solders. The sealing is carried out in vacuo using specially designed RF induction heaters. Both sealing surfaces are gold coated.

3.3.2 Glass sealants

Johnson Matthey JMI4600 silver-glass sealing paste is being evaluated at AWAM for both substrate bonding and as an alternative to solder alloys for window sealing. This material is reported to have excellent adhesion and low outgassing properties. Sealing is conducted in a belt oven at 375°C.

Vitta glass transfer tape has been successfully employed for the sealing of the glass-ceramic components of ERL custom packages.

3.3.3 Polymer resins

A range of polymer resin adhesives has been used throughout the project for substrate bonding and hermetic seals. These materials are generally not favoured for vacuum packaging because of high outgassing rates, but are useful for detector evaluation.

Leak-tight seals have been achieved with Varian Torr Seal resin, Epo-Tek H74 thermally conducting epoxy resin, and Plastalloy 915 package sealing resin. Epo-Tek 410LV conducting epoxy resin is used routinely for substrate bonding.

3.4 Infrared windows

3.4.1 Window materials

The window materials used in this project were zinc selenide and germanium. Zinc selenide windows for first generation detector packages were cut from Raytran ZnSe material, then polished and anti-reflection (AR) coated on both surfaces. The window sizes are 5 mm diameter x 1 mm thick for TO5 packages, and 12.5 mm long x 7.5 mm wide x 1 mm thick for Tekform platform packages.

Zinc selenide has now been replaced by germanium for all package investigations. Windows were cut from single crystal ingots prepared at the ERL crystal growing facility, and were polished and AR-coated in ERL. Commercial Cerac polycrystalline material was used in a brief programme initiated to establish a cutting and polishing capability within Australian industry. The window size for ERL custom packages is 26 mm diameter x 1 mm thick, whilst the 12.5 mm x 7.5 mm size was retained for both platform and DIL packages.

A suitable sputter-deposited metallisation was applied to the edge of windows for sealing purposes, usually in the form of a 1.5 to 2 mm wide sealing ring. This coating is required only for solder seals, and is not used for seals made with glass-based and epoxy resin seals.

3.4.2 AR coatings

In keeping with a low cost philosophy, simple anti-reflection coatings were used to give a window transmission of greater than 90% over the desired spectral band. A single quarter-wave AR-coating was applied to zinc selenide windows. The preferred coating material is thorium fluoride; however radiation hazard considerations led to initial selection of lead fluoride, which was rejected because of poor

mechanical properties, and finally to barium fluoride.

Zinc selenide windows coated with barium fluoride AR-coatings (both surfaces) were found to withstand reasonable mechanical and environmental abuse, adequate for use in experimental field equipment. The typical window transmission is 0.91 over the 8 to 14 µm spectral band and 0.82 from 1 to 20 µm.

Germanium windows were coated over both surfaces with a ZnSe-Ge-ZnSe-B_aF_2 multilayer AR coating. These windows withstand substantial abuse and are generally superior to zinc selenide for field applications. The window transmission is 0.93 over the 8 to 14 µm band, but is inferior to zinc selenide over a wider spectral band.

3.4.3 Window seals

For detector evaluation purposes, adequate leak-tight seals were achieved with polymer resins such as Plastalloy 915 resin, Torr Seal, and Epo-Tek H74 epoxy resin. A T05 single element detector package fitted with a zinc selenide window is illustrated in figure 10. The window was sealed with H74 resin.

All windows which were sealed with solder alloys were precoated on the sealing surface (a 1.5 or 2 mm wide strip at the edge of the window) with a suitable bonding metallisation. Good results were achieved with a sputter-deposited Ti-Pt-Au coating for zinc selenide, and a Ge-Ta-Au germanium. Leak-tight seals to gold-plated kovar lids were accomplished on a routine basis with 96Sn4Ag solder. Window sealing was carried out in a small vacuum chamber using RF induction heating. In order to avoid excess solder flow, it is desirable to scribe a fine line in the gold plating around the sealing area. A zinc selenide window is shown solder-sealed to a platform package in figure 11.

The sealing of germanium windows to the flat gold-plated kovar lids of DIL packages is under investigation at AWAM. The silver-glass seal is carried out under controlled temperature in a nitrogen atmosphere using a conventional belt oven. No metallisation is required on the window. Note, however, that a simple solder preform seal or a pressure diffusion bond are suitable options for DIL package lids.

3.5 Substrate bonding and lead attachment

Epo-Tech 410LV silver-loaded epoxy resin was used for bonding first generation detector substrates to package bases. The resin is applied as small droplets at the edge of the substrate. The substrate is accurately positioned with a locating jig and is allowed to settle on the resin under the weight of a small PTFE block. The block is recessed to avoid contact with detector elements. This light loading ensures a uniform gap of about 0.1 mm between substrate and base, sufficient to avoid detector fracture during evacuation.

In order to reduce outgassing in evacuated packages, a solder 'die bond' is used at ERL for second generation detectors. The rear surface of the substrate is sputter-coated with a tantalum-gold metallisation, and the bond is completed in vacuo using a pure indium solder preform. Other solders may be employed when there is danger of re-melt during the final package seal. However this problem does not occur with the ERL custom package.

The use of a silver-glass paste for die bonding is under investigation at

AWAM.

Standard 0.25 mm gold wire is employed for lead bonding at ERL. Thermo-compression ball bonding is used for experimental work with gold-based substrate metallisation in the authors' laboratory, whilst a conventional ultrasonic wire bonder is used for routine lead attachment (including all aluminium metallisation) in AEL.

3.6 Final package seals

Three different techniques for making final package seals are outlined below. The brief summary does not include resin seals or pumping tubes, both of which have been employed for experimental purposes.

3.6.1 Dimple sealing technique

Because of the difficulty of forming a reliable lid-to-base seal with platform packages, a dimple sealing technique was developed and used mainly for gas-filled operation at atmospheric pressure. The lid is sealed to the base with a suitable resin or solder, such as Torr Seal or 50In50Sn solder, prior to the final dimple seal.

A small dimple is pressed in the base of the platform package and filled with pure indium. A 0.75 mm diameter hole is drilled through the dimple and base. In order to increase pumping speed and avoid pellicle damage during pump down, a shallow slot is milled in the platform surface beneath the substrate.

Having completed the window, substrate and base seals, the package is inserted, upside down, in a locating jig, and installed in a small vacuum chamber. The chamber is provided with Barocell and semiconductor pressure gauges (the latter was developed at ERL) giving absolute pressure readings from 1×10^{-5} to 760 torr. After pump down, the chamber is isolated and gas admitted to the desired pressure. A minimum of two pumping cycles is desirable for special gases to ensure total removal of residual gas species (the first cycles need not be taken to atmospheric pressure, thereby conserving expensive gases such as xenon). The package is then sealed with a small solder tip, which is manipulated onto the dimple.

This technique was used for the xenon-filled platform package shown in figure 11. The method can be readily extended to other package designs, particularly those with flat lids, and the potential for vacuum sealing remains an attractive option.

3.6.2 RF and radiant heating techniques

Both RF induction and radiant heaters have been investigated at ERL. Miniature RF heating coils have proved extremely effective for window seals (see Section 3.4.3), and with careful design can be used for final package seals. However consistent problems with detector damage, presumably due to RF pick-up, led to preference for radiant heating for final seals.

A full scale vacuum packaging system was developed at ERL and is used for sealing ERL custom packages. The system contains a precision package holder which separately clamps the base and window during pump-down and outgassing, then brings the two components together for the final seal. Heating is provided by two quartz-halogen tungsten lamps fitted with aluminium reflectors. One lamp is broadly focussed on the

package for outgassing purposes, whilst the other heats the window during the sealing operation. Outgassing and sealing is monitored with thermocouple probes.

Successful vacuum seals have been achieved in the above manner using a 96Sn4Ag solder preform pre-melted onto the package sealing surface prior to evacuation. An example is shown in figure 12.

3.6.3 Rim weld seals

This method is under evaluation at AWAM for sealing flat gold-plated kovar lids onto ceramic DIL packages. The package is provided with a rim-weld ring, and the seal is accomplished by passing a high current through a small wheel which is made to travel along the edge of the lid. Packages sealed at AWAM have the window pre-sealed as described in Section 3.4.3 and are filled with dry nitrogen at atmospheric pressure.

An attractive feature of this technique is that the provision of a gold-plated weld rim enables consideration to be given to the use of solder preforms in lieu of a simple weld, thereby reducing the power required in the sealing operation.

A detector package sealed by rim welding is shown in figure 13.

3.7 Preferred package sealing technique

Based on the experience gained in this project, it is considered that the preferred package is a side-brazed ceramic package, similar to the DIL type used by AWAM for industry evaluation but optimised (in dimensions) for the particular detector substrate.

The window would be sealed to the flat lid in a conventional belt oven, as described in Section 3.4.3, and a rim weld technique would be used for the final lid-to-base seal. There appears to be no practical reason why the rim weld operation cannot be carried out in a vacuum chamber specially designed for that purpose, and it is conceivable that a belt-driven or carousel arrangement would enable a number of packages to be sealed during the same pump-down cycle. An optional approach is to use the dimple sealing technique for the final package seal.

4. DETECTOR RESPONSIVITY

4.1 Analysis of responsivity

The detector responsivity is, by definition

$$\mathcal{R} = V_S/P_S \qquad V.W^{-1} \tag{1}$$

where V_S and P_S are the rms values of the fundamental component of the signal voltage and signal power respectively.

For a thin film bolometer detector, it can be shown(ref.1) that

$$V_S = BIR\alpha\Delta T \tag{2}$$

and

$$\Delta T = \frac{\epsilon P_s}{G(1 + 4\pi^2 f^2 \tau^2)^{\frac{1}{2}}} \quad (3)$$

where
- ε is the emissivity of the detector
- $B = R_L/(R+R_L)$ is the circuit bridge factor
- I is the bias current
- R is the electrical resistance at bias of the detector element
- R_L is the series load resistance
- α is the temperature coefficient of resistance(TCR)
- ΔT is the incremental temperature rise following signal irradiation
- G is the total thermal conductance coupling the detector to its surroundings
- f is the frequency of signal modulation
- τ is the thermal time constant

Under steady bias conditions the detector will attain an average temperature T (K) above the ambient background temperature T_o, given by

$$T - T_o = P/G = I^2R/G \quad (4)$$

where P is the bias power, and it is assumed that the thermal conductance is constant over the temperature range T_o to T.

The responsivity can be determined directly from the measurement of signal voltage at a given signal power (equation (1)), and should be reported as a function of operating conditions, eg, bias current. The intrinsic responsivity is obtained by normalising the measured value to unit bridge factor and taking into account the spectral characteristics of optical components such as the detector window.

An indirect estimate of responsivity can be obtained by using Joule heating to simulate absorbed signal power. This is a simple and useful technique, but requires a measurement of detector emissivity.

Given the detector responsivity, other important parameters, such as temperature rise and thermal conductance, can be calculated from equations (2), (3) and (4).

4.1.1 Low frequency responsivity

The low frequency (dc) responsivity is given by equations (2) and (3)

$$\mathcal{R}_{DC} = BIR\varepsilon\alpha/G \quad (5)$$

$$= BI\varepsilon\beta \quad (6)$$

where

$$\beta = R\alpha/G \quad (7)$$

Now

$$R = R_o + R\alpha(T - T_o) \quad (8)$$

$$= R_o + \beta P \quad (9)$$

where R_o is the cold resistance (measured at temperature T_o) and P is the bias power. Thus the value of β can be obtained from a plot of detector resistance versus bias power.

Given measured values of ε and α, the thermal conductance, (average) bias temperature, and responsivity can be evaluated from equations (6), (7) and (8). Note that the absorption and temperature coefficient characteristics of the detector are well established(ref.1,2), and for any given detector the values of ε and α are known to an accuracy of about ± 5%.

4.1.2 Dependence of responsivity on detector parameters

From equations (4) and (5), the low frequency responsivity can be expressed in the form

$$\mathcal{R}_{DC} = B\alpha\varepsilon\sqrt{\frac{R(T - T_o)}{G}} \quad (10)$$

where it is again assumed that the conductance is temperature independent.

This expression highlights the importance of various parameters when the detector is biassed at optimum temperature. First, it is common practice to use a bridge factor, B, approaching the maximum value of unity (ie a constant current source). Secondly, the maximum emissivity of a self-absorbing metal film is 0.5, and a further increase can be achieved only by interferometric techniques. Thirdly, the detector resistance is constrained by the requirement for maximum emissivity (nominally 189 Ω per square), although the actual value may range from 100 to 500 Ω for first generation detectors, and up to 10 kΩ for second generation detectors. However, whilst the responsivity at constant bias temperature varies as $\sqrt{R}$, the detectivity is independent of resistance (see Section 6.5).

Given the above constraints on the attainable values of B, ε and R, it is evident that the magnitude of $\alpha/\sqrt{G}$ is of particular significance for metal film bolometers. Obviously it is important to achieve the optimum (theoretical) value of TCR, and this requirement has been the subject of extensive research at ERL. The thermal conductance is dependent on detector geometry, and the small values attained with ERL bolometers is a significant feature of the technology. The conductance is also strongly related to both the pressure and type of gas in the detector package.

4.2 Measurement of responsivity

Four methods were employed for the measurement of detector responsivity, as follows:

(a) Estimation from microradiometer scan records of thermal spread in detector elements.

(b) Conventional radiant responsivity measurement employing a chopped blackbody source at a known distance from the detector.

(c) Radiant responsivity measurement with optical gain, using an optical system with known characteristics.

(d) An electrothermal analogue technique using Joule heating of the detector element to simulate absorbed radiation.

The first method was used for brief evaluations of detector performance. Method (c) is, however, a particularly attractive technique for the measurement of MFB responsivity, since the irradiance at the detector is much larger than that attained with the standard measurement technique (b). An f/1 Cassegrain objective was developed for this purpose, and would give a signal gain of 500; however for reasons of expediency, the majority of responsivity measurements were made using the simpler conventional method, supported by results obtained from the electrothermal analogue technique.

4.2.1 Measurement of radiant responsivity

The infrared source was an Infrared Industries blackbody, modulated by a PAR Model 192 variable frequency light chopper. The signal power is given by

$$P_S = \frac{M\sigma\, A_S A_d}{\pi\, D^2} (T_S^4 - T_o^4) \qquad (11)$$

where

M = chopper conversion factor

σ = Stefan-Boltzmann constant

T_S = source temperature

T_o = background temperature

D = distance from source aperture to detector

A_S = area of source aperture

A_d = area of detector

For

M = 0.45 (square wave),

A_S = 0.2 cm^2 ($\frac{1}{4}$ inch aperture),

A_d = 0.01 x 0.0075 cm^2 (first generation detector),

D = 15 cm,

equation (11) gives

P_S = 3 nW for a 500K source
22 nW for a 800K source

The preferred source temperature is 500K; however, since metal film bolometers are broadband detectors, the magnitude of the source temperature is not critical. Given a typical detector noise level of 3 to 5 $nV.H_z^{-\frac{1}{2}}$, the signal power from a 500K source is too small to cover the full range of detector responsivity. Thus in order to ensure a sufficient signal-to-noise ratio, an 800K source temperature was employed for most measurements.

The detector was connected in series with a wire-wound load resistance, and bias current was applied from a filtered battery supply. Two methods were used to measure signal voltage:

(a) A low noise amplifier, followed by a PAR Model 114/116 signal conditioning amplifier and a PAR Model HR-8 lock-in voltmeter, with the chopper unit providing a modulation reference for the voltmeter.

(b) A low noise amplifier followed by a HP Model 3582A Spectrum Analyser.

Low noise amplifiers were developed at ERL, the latest version having a 1 dB noise figure at frequencies down to < 25 Hz, referenced to detector Johnson noise. The spectrum analyser method was recently introduced to facilitate the large number of measurements required for operational detector arrays.

Amplifier gain is calibrated by injecting a known voltage from a precision oscillator into the low noise amplifier input. The amplified rms output from the detector is then divided by the gain calibration factor to give signal voltage, and the responsivity is found from equation (1), using equation (11) to calculate the rms signal power.

The responsivity was usually measured at a frequency of 110 Hz. By varying the chopper speed a plot of responsivity versus frequency is obtained. Detector speed of response is calculated from this data, and extrapolation to zero frequency gives the dc responsivity. The same equipment was also used to measure detector noise, leading to calculation of detectivity (Section 6.1).

4.2.2 Electrothermal analogue techniques

This method makes use of Joule heating to simulate absorbed signal power, and relies on a linear relationship between temperature coefficient of resistance and temperature. The detector absorptance (or emissivity) must be known in order to calculate responsivity.

Both ac and dc bias circuits were used for the measurement of detector performance. For ac bias tests, the detector is connected in a Wheatstone bridge arrangement, one arm comprising the detector and load resistance, the other a precision decade shunt and matching load resistance. The voltage drops across the detector and shunt are applied to a Tektronix Type 3A9 differential amplifier and displayed on a Model 564B storage oscilloscope.

The decade shunt is adjusted to null the bridge against the cold resistance of the detector (this can be accomplished at low current and high amplifier gain). When a stepped bias current is applied to the

detector, a differential voltage, ΔV, is developed due to Joule heating of the detector element, and the waveform appearing on the oscilloscope is the thermal response characteristics of the detector. A typical example is shown in figure 14.

An estimate of the dc responsivity can then be made from

$$\mathcal{R}_{DC} = \Delta V/\varepsilon P \qquad (11)$$

The thermal time constant can be determined from the value corresponding to 0.632 ΔV observed on the oscilloscope trace.

The ac bias method provides a rapid test of responsivity and speed of response under a range of operating conditions. This technique was also used to test responsivity prior to and following package sealing. The value of ΔV is a measure of pressure over the range 1 mtorr to 1 torr.

A more accurate determination of responsivity is obtained from the I-V characteristics of the detector under dc bias. The plot of resistance versus bias power is in the form of equation (9), and the measured slope at a given power (and hence current) is used in equation (6) for the calculation of responsivity. A typical example is shown in figure 15.

4.3 Detector element characteristics

The responsivity was measured for both single element detectors and the individual detectors of 20-element linear arrays. Relevant characteristics of these detectors are given in Table 3.

TABLE 3. DETECTOR ELEMENT CHARACTERISTICS

Type	Element size (μm)	Pellicle size (μm)	Resistance (Ω)
First generation single element	100 x 100	500 (dia)	150 to 250
First generation array	100 x 75	100 x 300	250 to 500
Second generation array type A	70 x 70	200 x 200	1.5k to 2.5k
Second generation array type B	70 x 70	200 x 200	5.0k to 10k

Detectors of 50 μm size were also prepared, and a few larger detectors of size > 1 mm were fabricated during the project. First generation detector elements have a simple rectangular geometry, as shown in figure 2, which is dictated by the use of mechanical evaporation masks. Second generation detector elements are formed by photolithography, thus allowing a wider choice of dimensions. Type A and B detectors are a zig-zag (meander) design, as shown in figure 5, and have a conductor width of 20 μm and 10 μm respectively.

4.4 Vacuum responsivity

The total thermal conductance for a thin film bolometer operated in vacuo is the sum of radiation conductance and planar conductance (heat loss to nearby heat sinks in the plane of the detector film). For gas-filled packages there is an additional contribution due to gaseous conduction loss. Thus it is clear from equation (10) that the maximum responsivity for a given detector operated at optimum bias temperature is attained in vacuo, and the value measured at low frequency is a suitable performance reference.

4.4.1 First generation detectors

The typical values of low frequency responsivity for detectors operated in vacuo at optimum bias temperature are given in Table 4.

TABLE 4. TYPICAL VACUUM RESPONSIVITY OF FIRST GENERATION DETECTORS

Size (μm)	R_o (Ω)	$\mathcal{R}$ ($V.W^{-1}$)
100 x 100	150	35
100 x 75	350	50
100 x 50	500	70

Operating conditions: Bias temperature: 400K
Bridge factor : 0.95

In practice the responsivity of individual detectors of a given size varies over a limited range because of small changes in TCR and thermal conductance as a consequence of processing variations, acting in addition to deliberate changes in sheet resistance. For a 100 μm x 75 μm detector with a resistance of 350 Ω, the typical range is 45 to 55 $V.W^{-1}$.

It should also be noted that the responsivity given in Table 4 refers to broadband spectral performance, and must be corrected for the transmission characteristics of the package window.

The measured responsivity is in good agreement with theory(ref.1). However the maximum predicted value (50 $V.W^{-1}$ for a 0.1 mm x 0.1 mm detector) is not attained with first generation processing because the optimum TCR is not achieved.

4.4.2 Second generation detectors

The versatility of the second generation process enables the design of detectors which have a higher thermal efficiency. For example, the detector shown in figure 5 has a nominal element size of 70 μm x 70 μm, but the effective length for planar conduction loss is 200 μm, giving a lower value of planar conductance. In addition, it is possible to optimise annealing requirements, with a consequent enhancement in TCR. The result is a higher value of the parameter $\alpha/\sqrt{G}$ compared to first generation detectors.

Noting that the responsivity of detectors operated at the same bias temperature increases with the square of element resistance, the low

frequency vacuum responsivity for second generation detectors is much higher than that of first generation detectors. Typical values are given in Table 5.

TABLE 5. TYPICAL VACUUM RESPONSIVITY OF SECOND GENERATION DETECTORS

Size (μm)	R_o (kΩ)	$\mathcal{R}$ ($V.W^{-1}$)
70 x 70 (type A)	1.6	120
70 x 70 (type B)	5.5	220

Operating conditions: Bias temperature: 400K
Bridge factor : 0.85

4.5 Dependence of responsivity on gas pressure

When gas is admitted to the detector package, the consequent pressure rise is accompanied by an increase in thermal conductance and hence a decrease in responsivity. According to equation (5), when the detector is biassed at constant current the responsivity is proportional to the inverse of the conductance, whilst at constant temperature (equation (10)) the responsivity varies as the inverse square root of conductance.

The decrease in responsivity with increasing gas pressure is illustrated in the ac bias record of figure 16. The detector response is shown at four different pressures for nitrogen admission. Note also the increase in speed of response as the pressure is increased.

4.5.1 Dependence on gas type

The responsivity was measured as a function of pressure, from vacuo to 760 torr (atmospheric pressure, 1×10^5 Pa). Because the thermal conductance depends on the type of gas used in the detector package, a number of different gases were investigated. These included hydrogen, helium, air, nitrogen, argon, perfluropropane (C_3F_8), Freon-12 ($CC\ell_2F_2$), Freon-22 ($CHC\ell F_2$) and xenon.

Hydrogen and helium are of interest only for 'fast' detectors, the rapid speed of response being gained at the expense of decreased responsivity. Packaging also presents obvious problems with these gases. The responsivity of argon-filled detectors is higher than that for air and nitrogen, but the magnitude is not sufficiently great to warrant special attention, other than as a common gas preference. A significant increase in responsivity is achieved with perfluropropane, a gas originally thought to be attractive because of its low thermal conductivity; however common Freon refrigerant gases have equally desirable properties and are more suitable because of their lower boiling point temperatures. The highest responsivity is attained with xenon, and this gas is normally preferred, except when cost considerations outweigh the need for maximum performance.

These qualitative results are in agreement with the Part 1 predictions,

and led to the selection of four alternatives for gas-filled detectors operated at atmospheric pressure:

(a) Nitrogen as a reference gas.

(b) Argon for low cost detectors where maximum performance is not required.

(c) Freon-22 (which is slightly superior to Freon-12), where a higher performance is required at low cost.

(d) Xenon for maximum responsivity.

4.5.2 Measured responsivity as a function of pressure

The low frequency responsivity of a typical first generation detector is plotted as a function of pressure at constant bias current in figure 17. From this figure, the following general trends may be observed:

(a) The responsivity falls off rapidly from the maximum value attained in high vacuo when the pressure exceeds 0.01 torr (1.3 Pa).

(b) The responsivity approaches a constant value at pressures greater than about 100 torr (1.3×10^4 Pa).

(c) The responsivity of xenon-filled detectors is superior to that of other gases over the entire pressure range.

(d) There is little point in selecting gases other than xenon in preference to, eg nitrogen, for operation at pressures less than atmospheric.

These observations have important implications for detector packaging. First, it is necessary to maintain a pressure of only 1 mtorr in order to achieve the maximum vacuum responsivity. Secondly, if a detector is operated in the pressure range 0.1 to 10 torr (which may be desirable if outgassing cannot be avoided, but maximum responsivity is required), then only xenon offers a significant advantage over nitrogen or argon. Thirdly, Freon-22 would only be used at atmospheric pressure, and then only as a low cost alternative to xenon.

The ratio of vacuum responsivity to the responsivity in nitrogen at pressures greater than 100 torr was measured for a number of detectors under conditions of constant bias current, and lies in the range 9 to 14. The responsivity of Freon-12 and xenon-filled detectors, over the pressure range 100 to 760 torr, is respectively 1.5 to 1.7 and 2.0 to 2.5 higher than nitrogen-filled detectors operated at the same bias current.

4.6 Dependence of responsivity on bias temperature

According to equation (10), the responsivity is proportional to the square root of the bias temperature, which in turn increases with the square of the bias current. This relationship was found to apply for temperatures up to about 100K above ambient, eg approximately 400K. This is roughly the maximum safe bias temperature for stable operation (see Section 7.3), and is the normal bias condition chosen to achieve optimum responsivity.

The observed departure from the simple theory of responsivity (outlined in Section 4.1), which occurs at higher bias temperatures, is interpreted as failure of the assumption of constant thermal conductance. In this

regard, it should be noted that the experimentally determined bias temperature is an average value, and the actual temperature is not constant across the detector. It is shown in Part 1(ref.1) that the maximum temperature at the centre of a 100 μm bolometer detector is approximately 1.5 times the average value. It follows that the measured detector resistance must also be an average resistance.

The apparent (average) bias temperature can be calculated from the differential voltages measured in the pulse bias technique, ie

$$T - T_o = \frac{\Delta V}{BIR\alpha} \qquad (12)$$

However a more accurate estimate is obtained from the R-P characteristics of the detector under dc bias. From equations (4) and (7)

$$T - T_o = P\beta/R\alpha \qquad (13)$$

The calculated bias temperature for the first generation detector plotted in figure 17 is 400K, when the detector is operated in vacuo. The effect of increasing the pressure (at constant bias current) is to reduce the temperature. At 760 torr the bias temperature is 308K and 318K for nitrogen and xenon respectively.

Preliminary measurements indicate that second generation detectors can be operated at a substantially higher bias temperature than first generation detectors. This is a consequence of both improved detector design and a higher burn-out temperature (see Section 7.3). However, the relationship between responsivity and bias temperature is similar to that of first generation detectors, and the practice at ERL is to adopt the same bias temperature for normal operation.

4.7 Thermal conductance

The thermal conductance was calculated from either the measured value of responsivity or from the slope of the R-P bias plot, using equations (5) and (7) respectively.

The conductance for first generation detectors, derived from measurements made on a number of specimens over the temperature range 300 to 400K, is as follows:

G =	1.0 to 2.0 x 10^{-6} W.K^{-1}	Vacuo
	7.5 to 10.0 x 10^{-6} W.K^{-1}	Xenon at 100 torr
	1.0 to 1.5 x 10^{-5} W.K^{-1}	Freon-22 at 100 torr
	1.5 to 2.5 x 10^{-5} W.K^{-1}	Nitrogen at 100 torr

These values are substantially in agreement with theoretical predictions. Preliminary measurements on second generation detectors give similar results, but suggest that a reduction in conductance by a factor of 2 can be achieved in vacuo, with a subsequent $\sqrt{2}$ enhancement in responsivity.

4.8 Dependence of responsivity on bias current

According to equation (5), the responsivity should be linearly proportional to bias current, and hence it is desirable to employ the maximum possible current within the bounds of stable operation. Plots of responsivity versus bias current for a first generation detector are shown in figures 18 and 19. It is evident that a point is reached where the responsivity is no longer linearly dependent on bias current, and this point is found to correspond to a bias temperature approaching 100K above ambient (see also Section 4.6).

The departure from a linear current dependence is predicted from theory. However the stage where an increase in current produces no further increase in responsivity is not reached in practice due to the onset of detector instability (see Section 7.3).

The practical compromise adopted for 100 μm size detectors is to set the bias current to give an (average) bias temperature of about 400K, ie 100K above an ambient temperature of 290 to 300K. This means that a gas-filled detector is operated at a substantially higher current than a vacuum bolometer, thereby partly compensating for the higher thermal conductance. It is emphasised that the vacuum responsivity cannot be attained for any given gas-filled detector simply by increasing bias current, since it is clear from equation (10) that the responsivity of the evacuated detector will be greater by the ratio of the square root of thermal conductances. Thus the responsivity of a xenon-filled detector sealed at atmospheric pressure is at most $1/\sqrt{5}$ that of the same detector when evacuated and operated at maximum bias temperature.

4.9 Detector responsivity at optimum bias

4.9.1 First generation detectors

The dc responsivity of a typical first generation detector is given in Table 6. The table lists the bias current required for operation at a bias temperature of 400K. Bias power is also given, since this quantity is a guide to the desired current for detectors of similar design but different resistance.

TABLE 6. TYPICAL DC RESPONSIVITY OF FIRST GENERAL DETECTORS AT OPTIMUM BIAS

Gas type	Pressure (torr)	I (mA)	P (mW)	$\mathcal{R}$ ($V.W^{-1}$)
Vacuo	$\leq 10^{-3}$	0.65	0.16	50
Xenon	760	1.5	0.85	20
Freon-22	760	2.0	1.5	16
Nitrogen	760	2.5	2.4	12

Detector size: 100 μm x 75 μm
Detector resistance: 380 Ω
Bias temperature: 400K
Bridge factor: 0.95

The data in the table can be readily extrapolated for other operating conditions using equations (4) and (10).

4.9.2 Second generation detectors

The measured low frequency responsivity of a Type A second generation detector is given in Table 7.

TABLE 7. TYPICAL DC RESPONSIVITY OF A SECOND GENERATION DETECTOR AT OPTIMUM BIAS

Gas type	Pressure (torr)	I (mA)	P (mw)	$\mathcal{R}$ ($V.W^{-1}$)
Vacuo	$\leq 10^{-3}$	0.3	0.15	120
Xenon	760	0.7	0.8	50
Freon-22	760	0.8	1.0	40
Nitrogen	760	1.0	1.7	30

Detector size: 70 μm x 70 μm
Detector resistance: 1620 Ω
Bias temperature: 400K
Bridge factor: 0.85

Comparison of the data of Tables 6 and 7 shows that the responsivity of a second generation detector exceeds that which would be deduced from the respective values of detector resistance. This is because of the larger value of the parameter $\alpha/\sqrt{G}$.

5. SPEED OF RESPONSE

5.1 Measurement of speed of response

Detector speed of response (the thermal time constant) was determined in the usual manner from plots of radiant responsivity versus chopping frequency, ie

$$\tau = 1/2\pi f_c \qquad (14)$$

where f_c is the 3 dB cut-off frequency, when the responsivity falls to $1/\sqrt{2}$ of the maximum (dc) value.

Alternatively, the time constant was measured at the (1 - 1/e) intercept of thermal response records obtained with the ac bias technique described in Section 4.2.2. This is a powerful diagnostic method, since the detector can be mounted in a vacuum chamber and measurements made whilst admitting a selected gas under accurate pressure control. A typical example for an evacuated detector is shown in figure 14. The decrease in speed of response with increasing pressure is clearly illustrated in figure 16.

5.2 Experimental results

It was found that detector responsivity follows a simple exponential rise time law over a wide pressure range, extending from vacuo to at least 100 torr. The frequency response at atmospheric pressure departs from the simple form characteristic of a single unique time constant, because the gaseous thermal conductance and capacitance loading are frequency dependent. This departure at high pressure is observed as a more rapid fall in responsivity at low frequencies and a slower fall at high frequencies. An example is shown in figure 20, where normalised responsivity is plotted as a function of frequency for a detector operated in both vacuo and atmospheric pressure.

The typical speed of response of a 100 µm x 75 µm first generation detectors is given in Table 8.

TABLE 8. SPEED OF RESPONSE OF FIRST GENERATION METAL FILM BOLOMETER DETECTORS

Gas type	Pressure (τ)	Time constant (ms)
Vacuo	$\leq 10^{-3}$	1.0
Nitrogen	0.1	0.5
Nitrogen	760	0.15
Freon-22	760	0.2
Xenon	760	0.3

The values shown in Table 8 are characteristic of the speed of response of both first and second generation detectors which have an element size in the range 50 to 100 µm. Some minor differences are observed with different designs, eg, 0.7 to 1.5 ms for the speed of response in vacuo. By comparison, the measured time constant of a 2.5 mm long vacuum bolometer is 30 ms.

5.3 Thermal capacitance

The thermal self-capacitance of a detector can be estimated from the values of thermal conductance and time constant in vacuo, ie

$$\tau = C/G \qquad (15)$$

where C is the total thermal capacitance of the detector element and pellicle. For the detector response given in Table 8, the calculated capacitance is 1.5×10^{-9} $J.K^{-1}$, which is in good agreement with theoretical predictions.

Examination of the experimental data for a detector operated in nitrogen at atmospheric pressure shows that there is an effective capacitance loading of similar magnitude to the detector self-capacitance. In practice, however, the gaseous contribution to the total thermal capacitance decreases with frequency, whilst the conductance contribution increases.

This effect is explained in reference 1, and is responsible for the frequency response characteristics described above in Section 5.2.

6. DETECTOR NOISE AND DETECTIVITY

6.1 Measurement of detector noise

Detector noise was measured with the same signal analysis equipment employed for the measurement of radiant responsivity (Section 4.2.1). High performance lock-in voltmeters provide narrow band spot noise readings from which a noise spectrum can be compiled. Alternatively, a low noise amplifier can be used with a wave analyser, as described in reference 5.

Rapid noise measurements were made with a HP Model 3582A Spectrum Analyser, in conjunction with a low noise amplifier developed at ERL. The analyser provides a display of the noise spectrum, and the noise level is measured in absolute voltage units. Wire-wound resistors were used as detector references.

6.2 Excess noise

It was predicted in Part 1(ref.1) that the ultimate performance of an MFB detector would be limited by the Johnson noise of the detector resistance, except at very low frequencies where current noise should predominate. Earlier measurements failed to detect current noise above the level present in the best available electronic preamplifiers. However, the development at ERL of an ultra-low-noise amplifier, which has a noise figure of 1 dB at < 25 Hz referenced to detector Johnson noise, revealed an unexpected level of excess noise for both first and second generation detectors.

Additional noise was present as both current noise and white noise. After subtracting out the white noise and amplifier noise components, the noise voltage was found to be proportional to $I/\sqrt{f}$, and is thus readily confirmed as current noise.

A spectrum analyser record of a noisy first generation detector is shown in figure 21(a). The lower trace refers to the non-biassed condition, and therefore represents amplifier noise and detector Johnson noise. The upper trace applies to the biassed condition, and clearly shows additional white noise and current noise. A total noise figure of 30 dB was observed in the worst cases.

6.2.1 Origin and reduction of excess noise

Investigations have shown that most of the additional noise originates at detector contacts. It is believed that the current noise component is associated with non-ohmic behaviour, eg a Schottky barrier, whilst contact resistance (giving rise to shot noise) is responsible for the white noise contribution. A substantial reduction of noise was achieved with first generation detectors by paying special attention to contact metallisation, in particular by avoiding excessive heating during sputter etching of interconnects, and minimising contamination at the interface with the gold film detector contacts. In this manner it has been shown possible to reduce excess noise to a small 1/f contribution below 50 Hz.

It was found that poor adhesion of aluminium contact metallisation coincided with high levels of excess noise, presumably as the result of contamination or oxidation at the detector-contact interface. Detectors with strongly bonded metallisation, which were subjected to annealing

cycles up to 450°C, were virtually free of additional noise, as shown in figure 21(b).

Removal of parasitic noise sources reveals the intrinsic current noise of the detector element. For an evacuated detector operated at optimum bias temperature, the current noise is equal to Johnson noise at a frequency of about 5 Hz. The same (3 dB) noise level is observed at 10 Hz for gas-filled detectors because of the higher bias current.

6.3 Piezoresistance noise

Piezoresistance is the change in resistance caused by the application of mechanical stress, and will be evident in thin film bolometers as microphonics, ie an output voltage fluctuation associated with mechanical vibration. A qualitative test of the level of noise induced by microphony was conducted by sharply striking the detector package. For first generation detectors this produced a momentary doubling of the noise level.

Thin film bolometers can be designed for low microphony(ref.1). Whilst no special effort has been made in this direction, second generation detector design incorporates self-compensation features which reduces the level of piezoresistance noise.

No problems have been experienced with microphony in field radiometric applications. It is expected that this source of noise can be kept at a low level even under severe vibration conditions.

6.4 Noise limited performance

It is concluded that the detective performance of metal film bolometers is limited by the Johnson noise of the detector resistance at frequencies greater than 25 Hz. Current noise predominates at lower frequencies, and contributes 3 dB of noise at a frequency of 5 to 10 Hz. Parasitic noise sources can be reduced below the combined level of intrinsic current noise and Johnson noise. It can be shown(ref.1) that temperature-fluctuation-noise is at most $\frac{1}{4}$ that of Johnson noise.

The value of Johnson noise to be used in the calculation of detectivity is given by

$$V_J^2 = 4k \frac{R R_L}{(R + R_L)^2} (RT_o + R_L T) \qquad (15)$$

where k is the Boltzmann constant.

At frequencies less than 25 Hz, the total noise is the rms sum of Johnson and current noise.

6.5 Detectivity

The detectivity was determined from

$$D^* = \frac{\mathcal{R}\sqrt{A}}{V_n} \qquad (16)$$

$$= \frac{\sqrt{A}}{P_n} \qquad (17)$$

where V_n is the total detector noise, given for unit bandwidth ($V.Hz^{-\frac{1}{2}}$),

and P_n is the noise equivalent power ($W.Hz^{-\frac{1}{2}}$). The maximum detectivity was calculated from low frequency values of responsivity and Johnson noise estimated from equation (15). The typical maximum detectivity of ERL detectors is given in Table 9.

TABLE 9. MAXIMUM DETECTIVITY OF MFB DETECTORS

Detector type	R_o (Ω)	V_n ($nV.Hz^{-\frac{1}{2}}$)	P_n ($W.Hz^{-\frac{1}{2}}$)	D^* ($cm.Hz^{\frac{1}{2}}.W^{-1}$)
First generation:				
Vacuo	380	3.0	6.0×10^{-11}	1.4×10^{8}
Xenon (760 torr)	380	3.0	1.5×10^{-11}	5.8×10^{7}
Nitrogen (760 torr)	380	3.0	2.5×10^{-10}	3.5×10^{7}
Second generation:				
Vacuo	1620	5.6	4.7×10^{-11}	1.5×10^{8}
Xenon (760 torr)	1620	5.6	1.1×10^{-11}	6.2×10^{7}
Nitrogen (760 torr)	1620	5.6	1.9×10^{-10}	3.7×10^{7}

Detector size: First generation 100 µm x 75 µm
Second generation 70 µm x 70 µm

Bias temperature: 400K

In practice, the maximum detectivity is attained at a frequency of > 25 Hz, depending on the speed of response. At low frequencies the detectivity decreases because of current noise, whilst at higher frequencies the detectivity falls off in accordance with the response characteristics of the particular detector. This relationship is illustrated in figure 22 for both evacuated and gas-filled detector operation.

6.5.1 Comments on second generation performance

The higher detectivity of second generation detectors is a consequence of the enhanced value of the parameter $\alpha/\sqrt{G}$. However the data given in Table 9 refers to the first developmental batch of detectors, for which the enhancement factor is only 1.2. In particular, the optimum TCR (measured in the laboratory on test specimens) has not yet been achieved with fully processed detectors. Other factors which should be taken into account are:

(a) The bridge factor (determined by the test equipment) is lower for the second generation detector measurement because of the higher bolometer resistance, thereby reducing both the responsivity and detectivity by a factor of 1.11.

(b) The area of the second generation detector element listed in Table 9 is smaller than that of the first generation detector, with the result that the detectivity (equation (16)) is reduced by an additional factor of 1.24.

(c) Second generation detectors can be operated at a higher bias power, with a consequent gain in both responsivity and detectivity.

An increase in TCR by a factor of up to 1.7 has been demonstrated in laboratory measurements, and has been achieved with fully processed low-resistance (ie thicker) detector elements. It is anticipated that an enhancement in the parameter $\alpha\sqrt{G}$ of about 2 can be realised with further development of the technology. The attainable D* of a 50 to 100 µm sized detector, prepared by the second generation process, is 3×10^8 cm.Hz$^{\frac{1}{2}}$.W^{-1} in vacuo, and 1×10^8 cm.Hz$^{\frac{1}{2}}$.W^{-1} when xenon-filled at atmospheric pressure.

7. BIAS LIMITATIONS AND OPERATIONAL TESTING

7.1 Testing of detector resistance

The resistance of all first generation detectors was measured immediately after processing. In the case of arrays, the resistance of each detector element was measured with a microcircuit wire probe and the values plotted on a pen recorder. Spot probe tests were made on second generation detectors prior to wafer separation. Selected arrays were then subjected to the full probe testing adopted for first generation detectors.

Detectors were selected for packaging on the basis of both resistance records and visual inspection. In addition, the TCR was measured of representative samples of each process batch. The resistance was measured after wire bonding, and again after packaging, both before and after bias current testing. In this manner, a complete history was recorded for each detector, showing every stage of processing.

The typical spread in resistance for first generation arrays was ± 10%. This spread includes a systematic drop in resistance along the array, which results from a masking deficiency, and can be corrected. A spread of ± 5% is expected for production runs.

A resistance spread of 2% is typical with second generation arrays, and in most cases the spread does not exceed 5%. However the value of the resistance of different arrays prepared on the same 3 inch wafer varies by up to 15%. This is a consequence of the need to keep the wafer stationary during detector film deposition, and hence ensure a thin step coverage desired for the lift-off process. Deposition under planetary motion reduces variation across the wafer, and is preferred for plasma-etched detectors or bi-layer lift-off processing.

Particular care must be taken, when measuring detector resistance, to avoid the application of excessive test currents. Special test circuits were developed at ERL for deposition control and probe measurement, which apply a typical test current of 20 µA. Digital voltmeters such as the Kiethley Models 160B and 179A were used for routine measurement of the resistance of packaged detectors. Conventional ohmeters and many DVMs employ high test currents, and will either destroy the detector being measured or, at best, give false readings due to Joule heating.

7.2 Bias current testing

All packaged detectors were subjected to thorough bias testing prior to use in infrared detection systems. A 'burn-in' test box was constructed for detector arrays, which makes provision for the simultaneous application of bias current to all detectors in the array. Terminals are provided for

the measurement of cold resistance and bias voltage. The resistance under bias is then readily determined from the set value of the bias current.

Having determined the desired bias condition from responsivity data, a test current is applied which is typically 25% higher than the chosen operational value. An initial drop in resistance is usually observed, followed by gradual settling to a stable condition (normally within a few hours). In most cases the initial fall in resistance is small, but a significant change has been observed for those detectors which are suspected to have an excessive contact resistance. The detector is deemed to pass the bias test when the resistance remains stable for a minimum period of 1 day.

7.3 Bias current limitations

The maximum acceptable bias current for a given detector is determined by the onset of bias instability, which is observed as a gradual rise in resistance at the set current (in addition to the rise due to temperature coefficient). A further increase in bias current leads to a rapid rise in resistance and subsequent burnout.

In agreement with the predictions of Part 1(ref.1), it was confirmed that electromigration is the principle cause of failure in first generation detectors. This phenomenon was demonstrated by slowly increasing bias current to the stage where the resistance (at a given current) began to rise, then removing the bias before failure occurred. Electromigration was then observed as mass depletion perpendicular to the current flow. The visual appearance is similar to thermomigration described in Part 2(ref.2), where failure in first generation detectors was found to originate from interdiffusion between the detector and gold film contacts during annealing cycles.

Thermomigration failure in first generation detectors occurs at a temperature of about 350°C, whilst electromigration failure takes place when the average temperature exceeds 200°C. This is not an unexpected result, since the two mechanisms are clearly related.

These observations suggest that a higher bias current could be applied with a different contact metallisation. Second generation detectors, which have aluminium metallisation, can in fact withstand higher bias currents (at a given resistance) than first generation detectors, and can be safely annealed at a temperature of at least 450°C.

7.3.1 Burnout current

The burnout current has been measured as a function of the pressure of the encapsulating gas for both first and second generation detectors, and the results are given, together with the respective bias power and approximate average temperature rise, in Table 10.

TABLE 10. BURNOUT CURRENT FOR MFB DETECTORS

Detector size (μm)	Pressure (torr)	R_o (Ω)	I (mA)	P (mW)	T_1 (K)
100x75 (first generation)	$\leq 10^{-3}$ 760 (N_2)	380	1.0 4.0	0.4 6.5	200 300
70x70 (second generation)	$\leq 10^{-3}$ 760 (N_2)	1600	0.43 2.0	0.5 8.5	300 400

Given the data in Table 10, it is possible to calculate the burnout current for detectors of different resistances, and for various gas-filled packaging. For example, the burnout current for a 380 Ω first generation detector packaged in xenon at 760 torr is 2.5 mA.

7.3.2 Long term failure tests

The data in Table 10 provides a guide to the maximum short term bias current. Burnout will occur if the values given in the table are exceeded for a period of the order or greater than the detector time constant. However, electromigration is a time dependent phenomenon, and failure may eventually occur at a lower current than that which causes rapid burnout.

Long term experiments were conducted to determine the conditions for an acceptable MTBF (Mean Time Between Failure). A summary of the results are as follows:

(a) A 100 μm x 100 μm first generation detector of 200 Ω resistance was biased at 2.5 mA in air for 2000 hours with no appreciable change in resistance.

(b) 75 μm x 100 μm detectors of 300 to 400 Ω resistance were subjected to steadily increasing bias currents in vacuo. There was no significant change in resistance after 50 hours of continuous operation at 0.65 mA. However, when biased at 0.75 mA, the resistance was observed to rise at a rate of about 3 Ω every 10 hours, followed by a rapid increase in resistance and sudden failure after 100 hours of operation.

(c) 75 μm x 100 μm (gas-filled) detectors have been operated for long periods in infrared detection equipment, with the bias current set to give an estimated temperature of 100 K above ambient.

From these results it has been established that ERL detectors can be safely biased at approximately 60% of the burnout current. Detectors can be operated at up to 75% of the instantaneous burnout current with a substantial reduction is lifetime.

The data given in Tables 6 and 7 provides a guide to the conditions for an acceptable MTBF, typically exceeding 1000 hour detector life.

7.4 Transients

Detectors which are operated under optimum bias conditions will withstand the normal abuse expected with ruggedised field equipment. However, care must be taken to avoid excessive current surges, particularly transients

originating from the bias voltage supply.

Detector failures have been traced to switching transients in the bias power supply, high current surges during lead bonding, electrostatic pickup, and pickup from RF induction coils during package sealing. Very short duration transients have been observed to cause an open circuit with no visual sign of damage, whilst large current surges lead to total detector destruction.

Damage arising from external sources can be minimised by employing suitable electronic design, taking conventional shielding precautions, and by paying careful attention to processing equipment, eg adequate earthing.

8. SUMMARY AND CONCLUSIONS

In this series of Technical Reports, we have given an account of the development at ERL of thin metal film resistance bolometer infrared detectors. Both single element detectors and 20 element linear arrays are now prepared on a routine basis. The detectivity of a 50 to 100 μm size detector is $\geq 1.5 \times 10^8$ cm.Hz$^{\frac{1}{2}}$. W^{-1} in vacuo, whilst for gas-filled detectors operated at atmospheric pressure, the detectivity is 6.2×10^7 and 3.7×10^7 cm.Hz$^{\frac{1}{2}}$. W^{-1} for xenon and nitrogen respectively. The respective speeds of response are 1.0, 0.3 and 0.15 ms.

Detectors are prepared on conventional semiconductor-grade silicon substrates, and extensive use is made of state-of-the-art microcircuit fabrication techniques. A method of preparation has been developed which employs wholly on-the-plane photolithographic processing, and this advanced second generation process is now established in the Australian microelectronic industry. In addition to the low inherent cost of manufacture, the technology forms the basis for further detector development, such as high performance semiconductor bolometers(ref.6) and other types of thin film thermal detectors. The 'stretch' potential of the second generation process also includes on-chip and hybrid signal processing.

Detectors are routinely sealed in xenon-filled microcircuit packages at ERL. Vacuum sealing of custom in-house designed packages has been demonstrated at ERL, and a low cost nitrogen-filled microcircuit packaging technique has been developed in industry. All packages are fitted with anti-reflection coated infrared-transmitting windows.

In the event of future applications which require evacuated or xenon-filled detector packages, it will be necessary to transfer ERL vacuum sealing technology to industry. It is considered that this can best be accomplished by adapting the ERL vacuum sealing system to industry requirements and locating the equipment with the detector manufacturer.

At the present stage of development, the full detective performance of the second generation process has not been achieved, mainly because the maximum temperature coefficient of resistance measured on laboratory test specimens is not attained with fully processed detectors. This is a materials problem, which should be resolved with further processing improvements.

The predicted detectivity of 70 μm size, enhanced-performance second generation metal film bolometer detectors, is 3×10^8 cm.Hz$^{\frac{1}{2}}$ W^{-1} in vacuo, and 1×10^8 cm.Hz$^{\frac{1}{2}}$ W^{-1} when xenon-filled at atmospheric pressure.

9. ACKNOWLEDGEMENTS

The authors wish to thank colleagues in Night Vision Group of Electronics Research Laboratory for many valuable contributions to detector development. They also express their appreciation to the staff of Electronics Work Group and Mechanisms and Instrumentation Group of Advanced Engineering Laboratory for support throughout the project.

The assistance given by AWA Microelectronics, Sydney, NSW, is also gratefully acknowledged.

REFERENCES

No.	Author	Title
1	Liddiard, K.C.	"Metal Film Bolometer Detectors : Part 1 - Introduction and Theory". ERL-0267-TR, March 1983
2	Liddiard, K.C. and Hlava, J.	"Metal Film Bolometer Detectors : Part 2 - Materials Research". ERL-0000-TR (In Publication)
3	Liddiard, K.C.	"An Improved Infrared Radiation Detector". Australian Patent 75842/81, 17 September 1981; Europe 81902611-3, 17 September 1981; Canada 386 338, 21 September 1981; USA 387 852, 21 May 1982; Japan 503059/1981, 17 September 1981
4	Liddiard, K.C.	"Thin Film Resistance Bolometer Infrared Detectors". IR Physics, Vol.24, No.1, p.57 January 1984
5	Rice, B.W.	"Assessment of the Performance of Low Noise Preamplifiers for Infrared Bolometer Detector Arrays". ERL-0000-TM (In Publication)
6	Liddiard, K.C.	"Development of a High Performance Thin Film Semiconductor Bolometer Detector". ERL-0000-TM (In Publication)

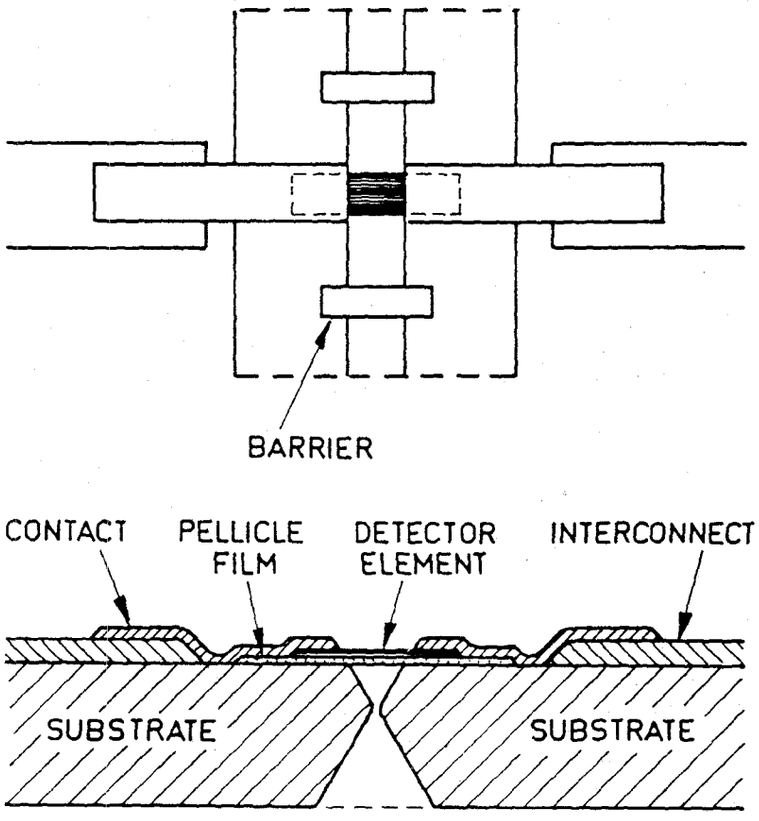

METAL FILM BOLOMETER ARRAY

SHOWING ONE DETECTOR ELEMENT WITH BARRIERS
SILICON SUBSTRATE (100) ORIENTATION

Figure 1. Cross-sectional schematic of a first generation detector

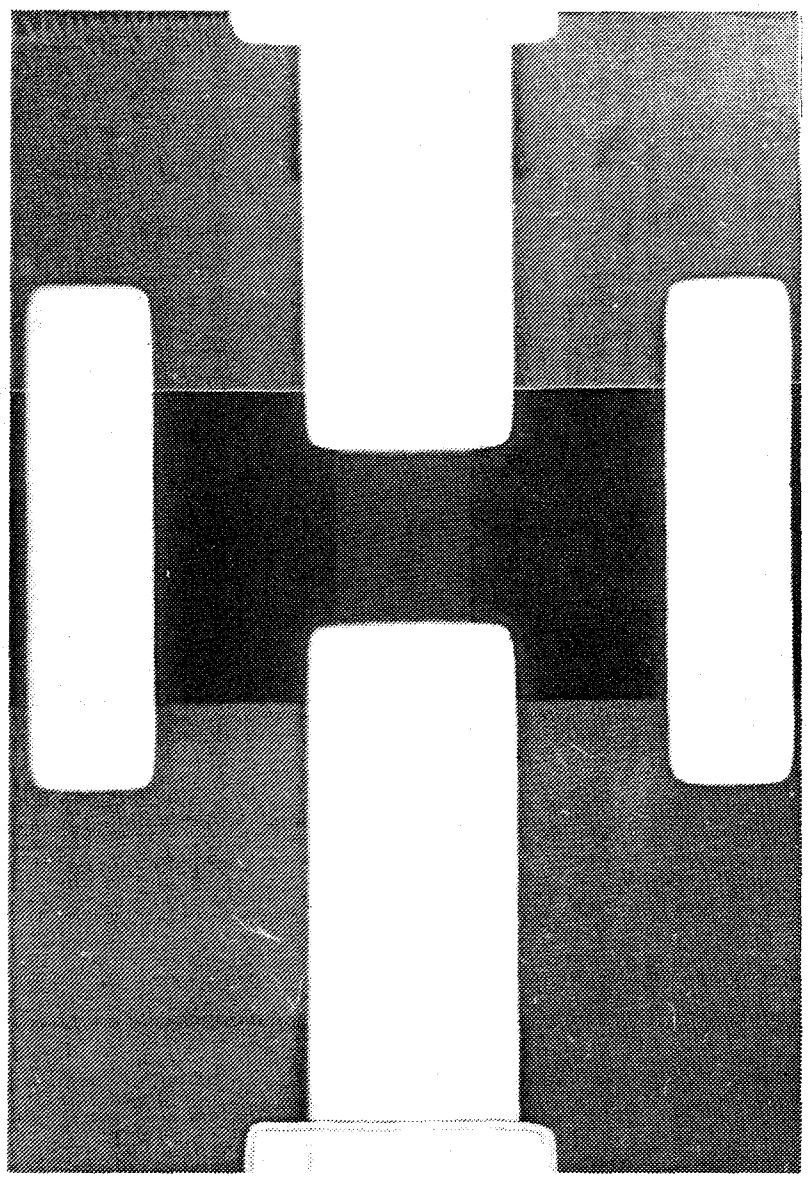

Figure 2. Microphotograph of a first generation detector

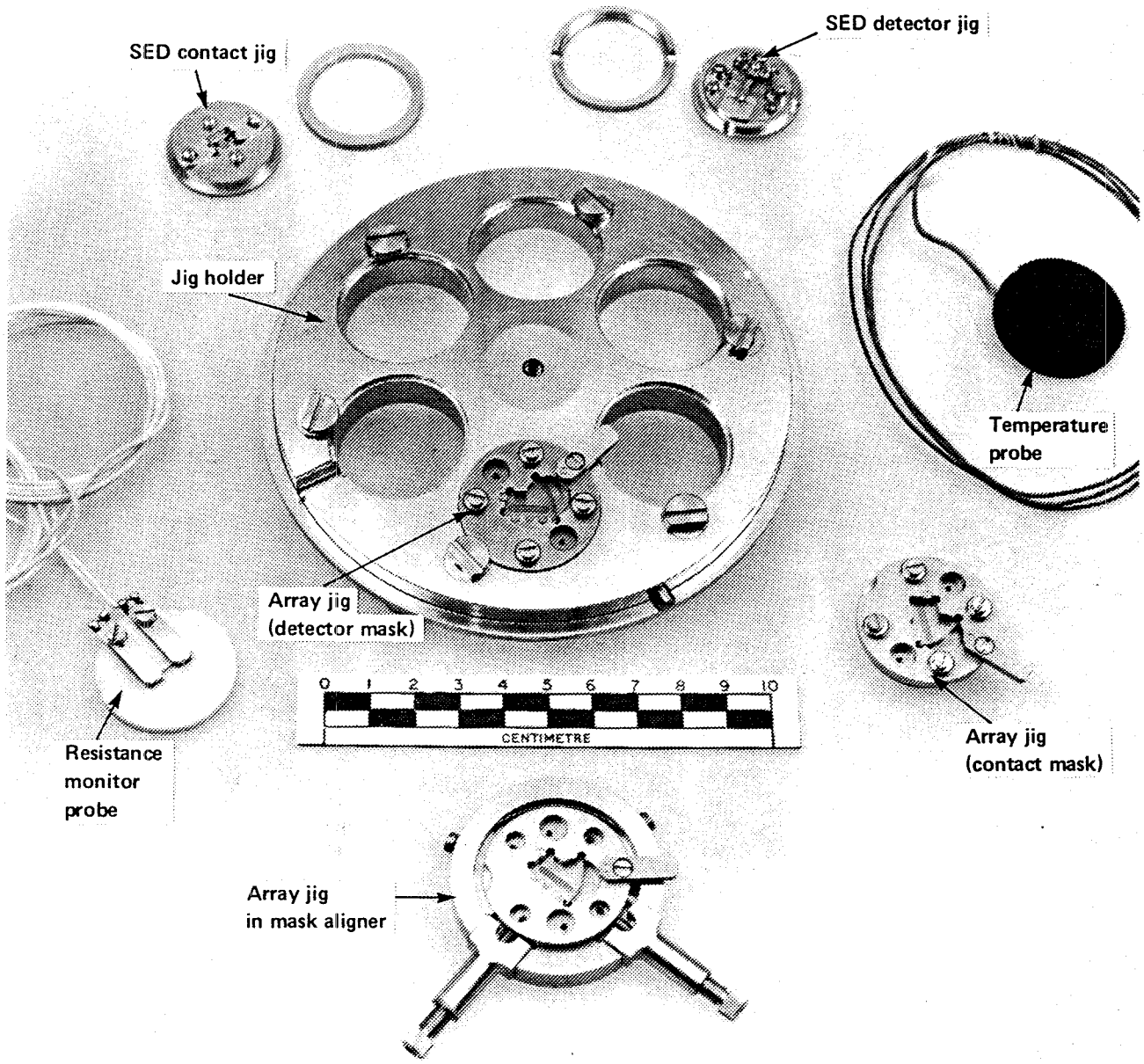

Figure 3. Vacuum deposition jigs

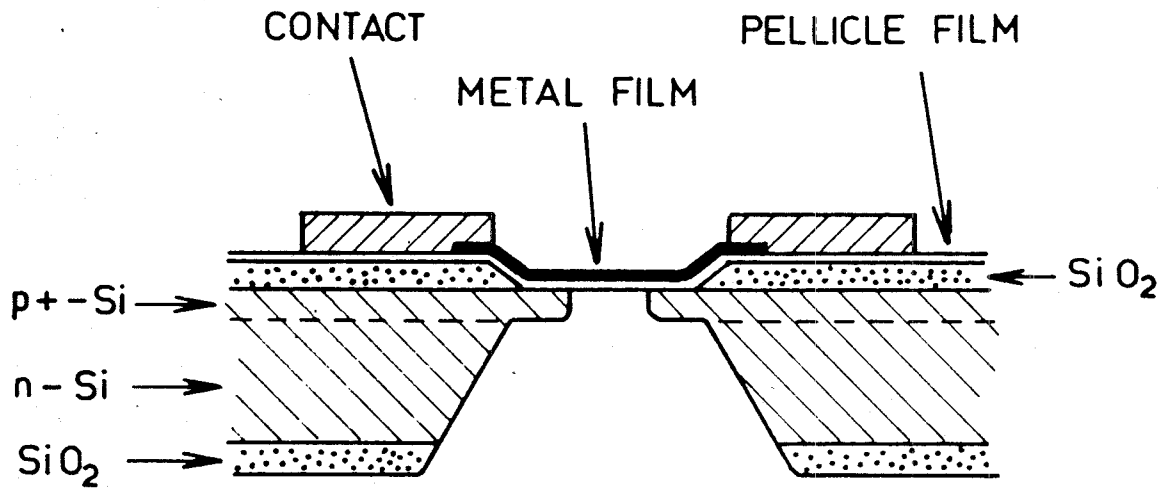

Figure 4. Cross-sectional schematic of a second generation detector

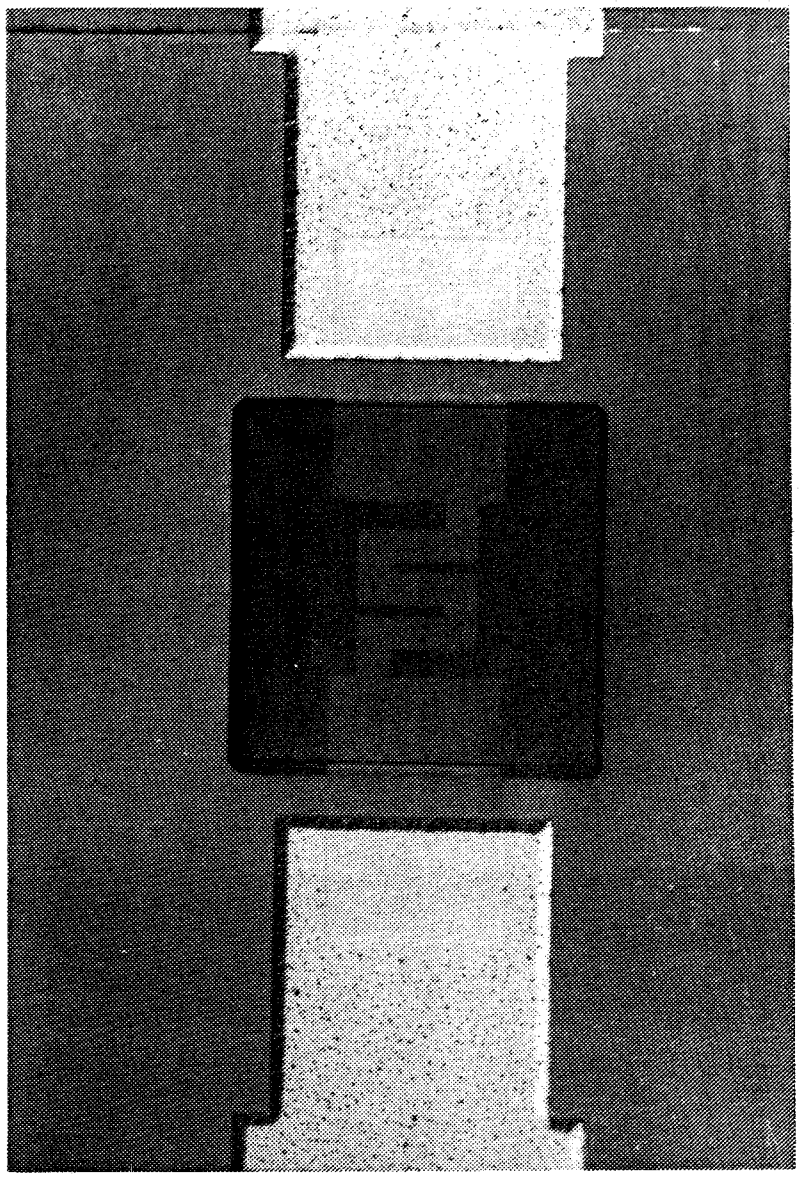

Figure 5. Microphotograph of a second generation detector

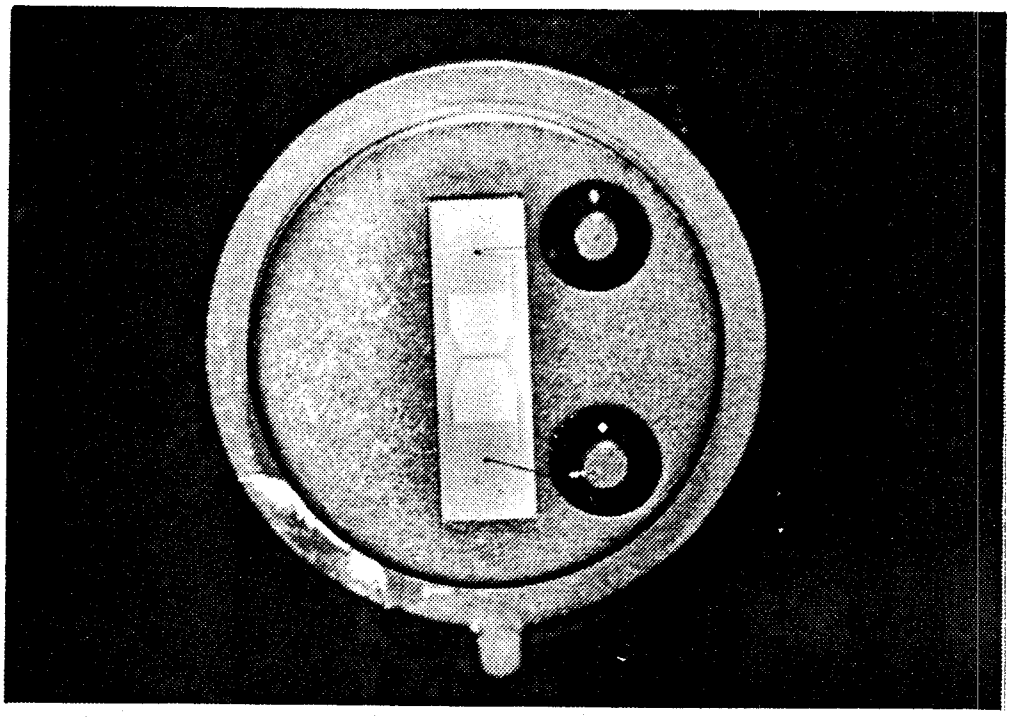

Figure 6. Single element detector mounted on TO5 header

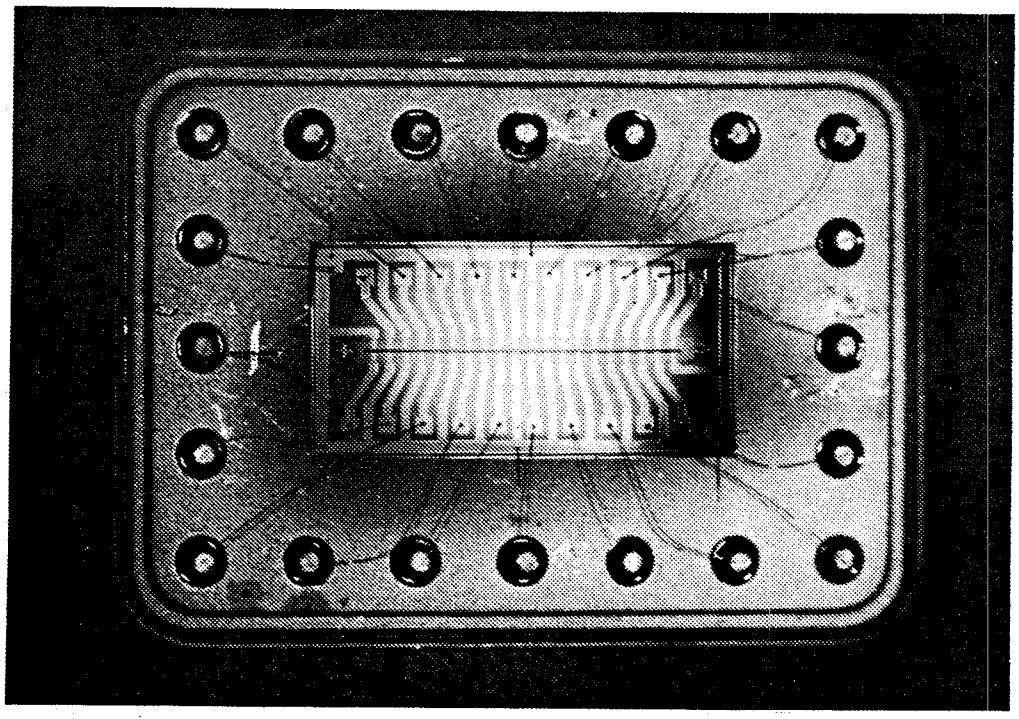

Figure 7. Detector array mounted on Tekform platform package base

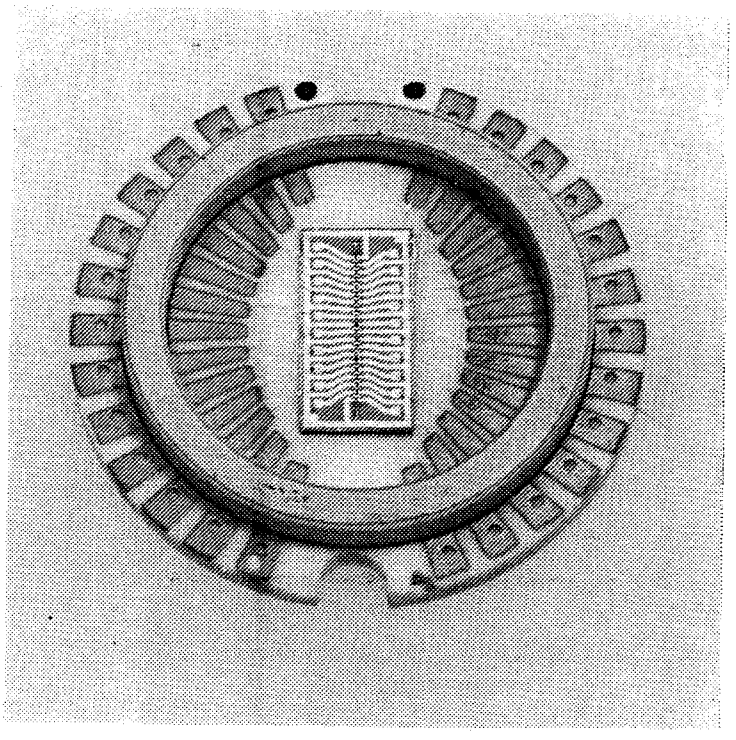

Figure 8. Detector array mounted in ERL package

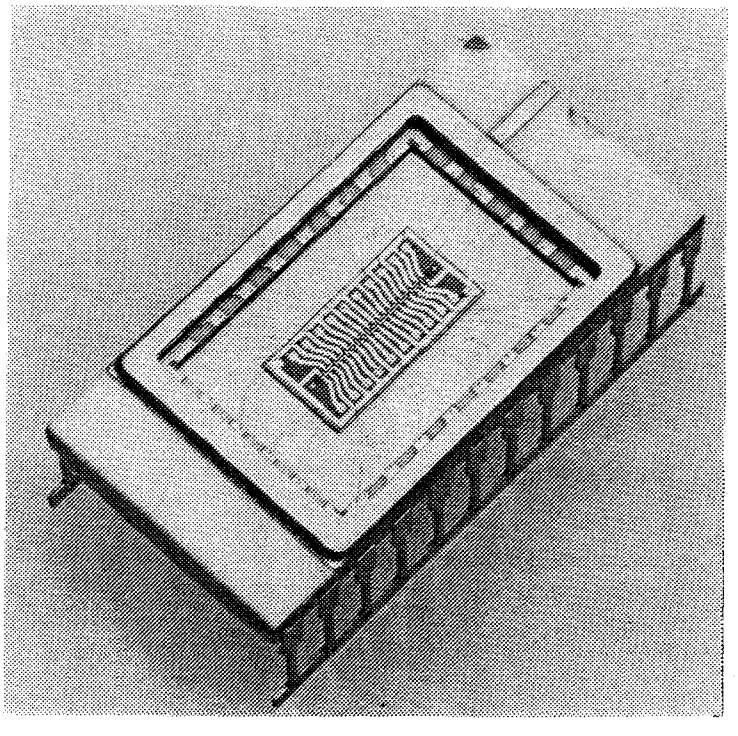

Figure 9. Detector array mounted in a DIL ceramic package

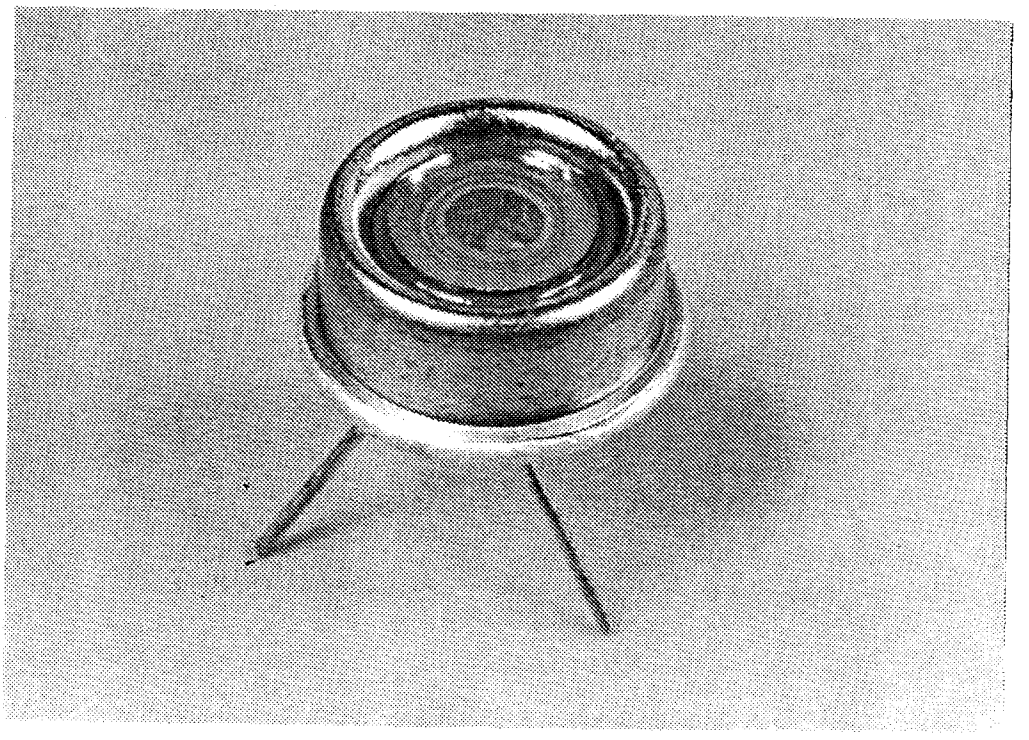

Figure 10. Single element detector package with zinc selenide window

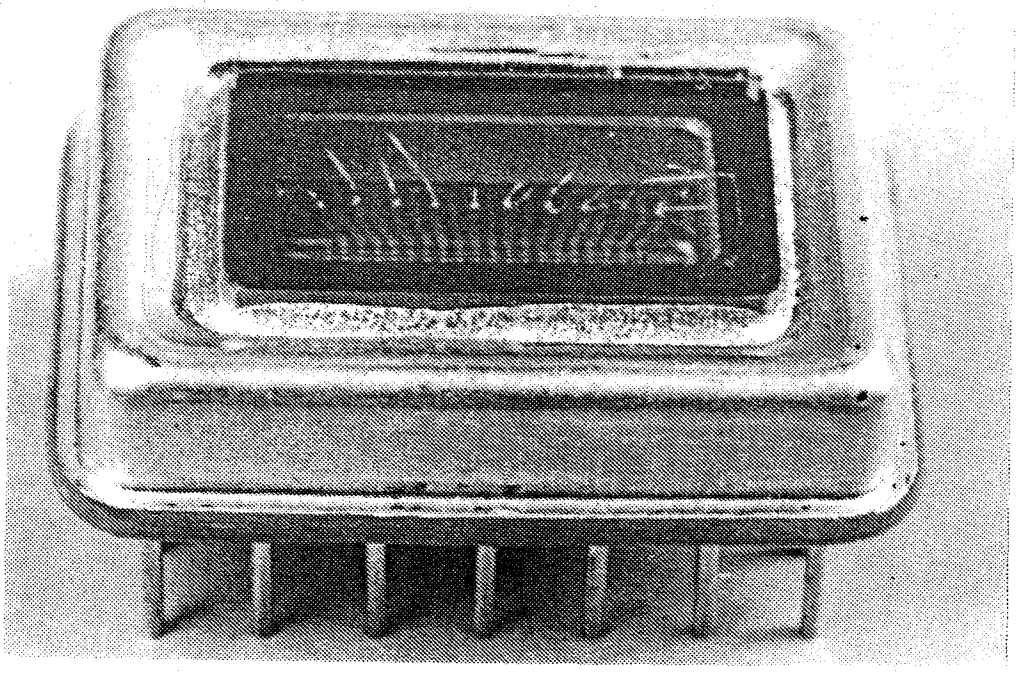

Figure 11. Tekform platform package with zinc selenide window

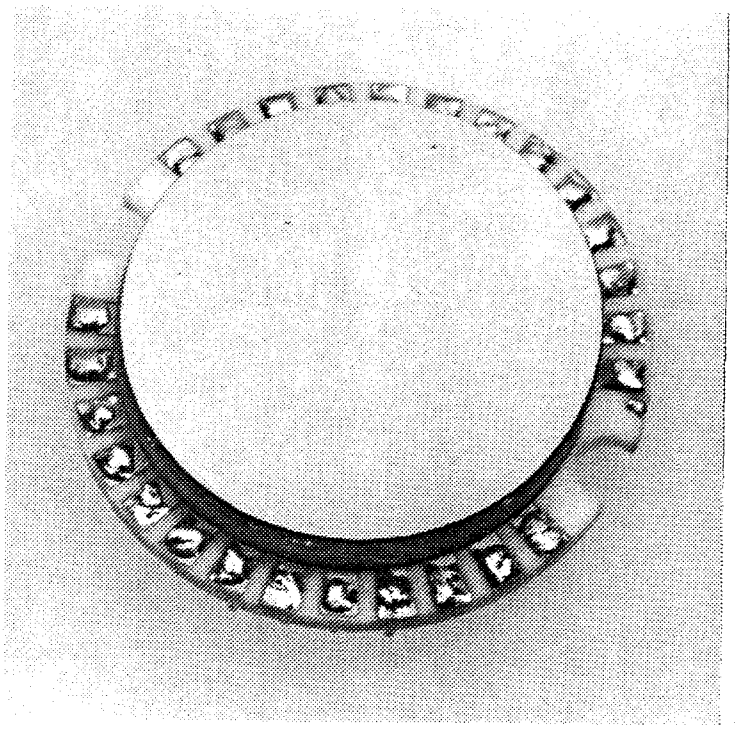

Figure 12. ERL custom package sealed in vacuo

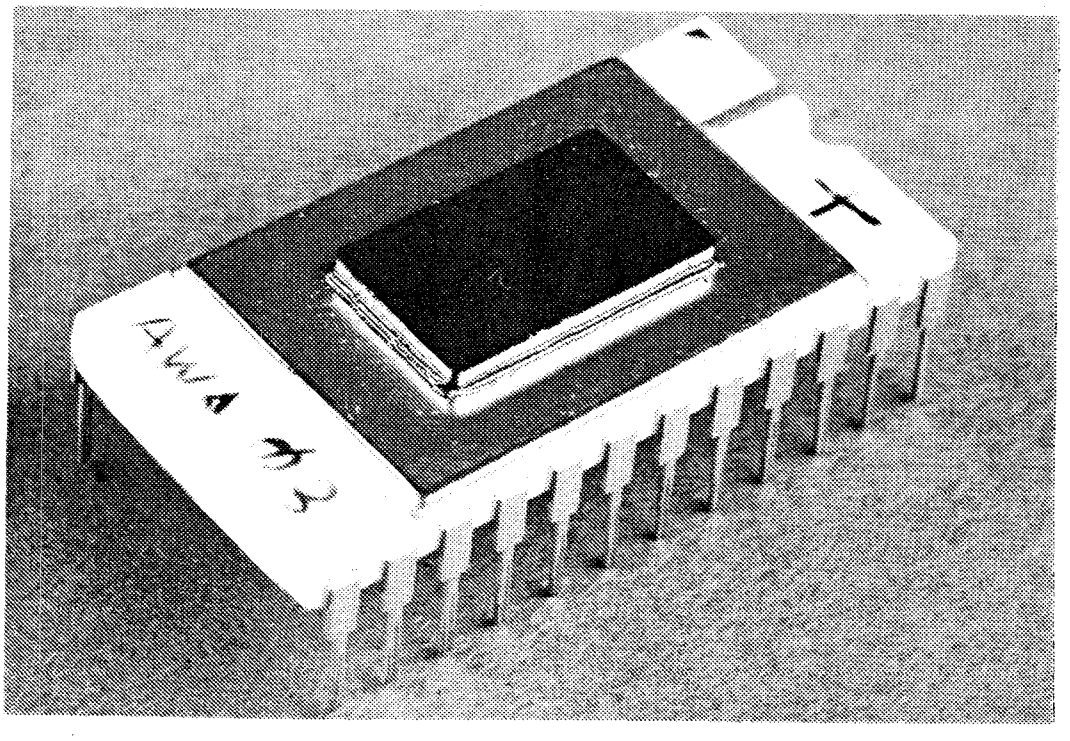

Figure 13. DIL ceramic package sealed by rim weld method

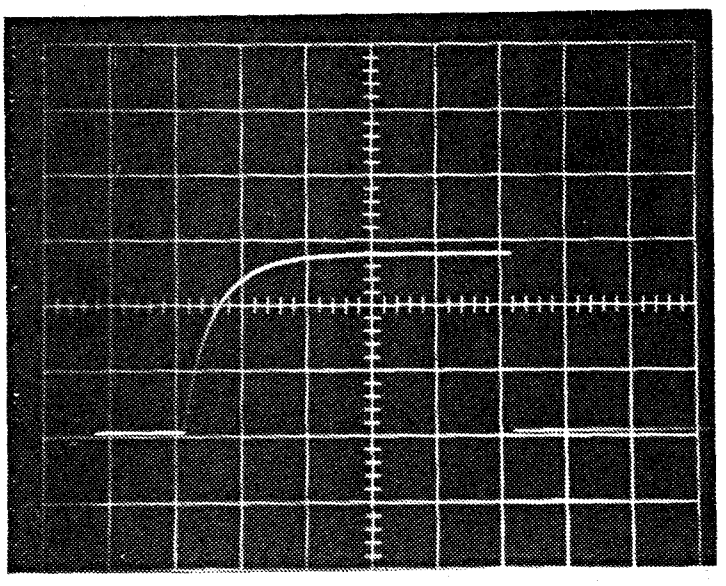

Specimen 68/2
X-axis 2 ms/div
Y-axis 10 mV/div
Vacuo

Figure 14. Thermal response characteristics of a first generation detector to a thermal step

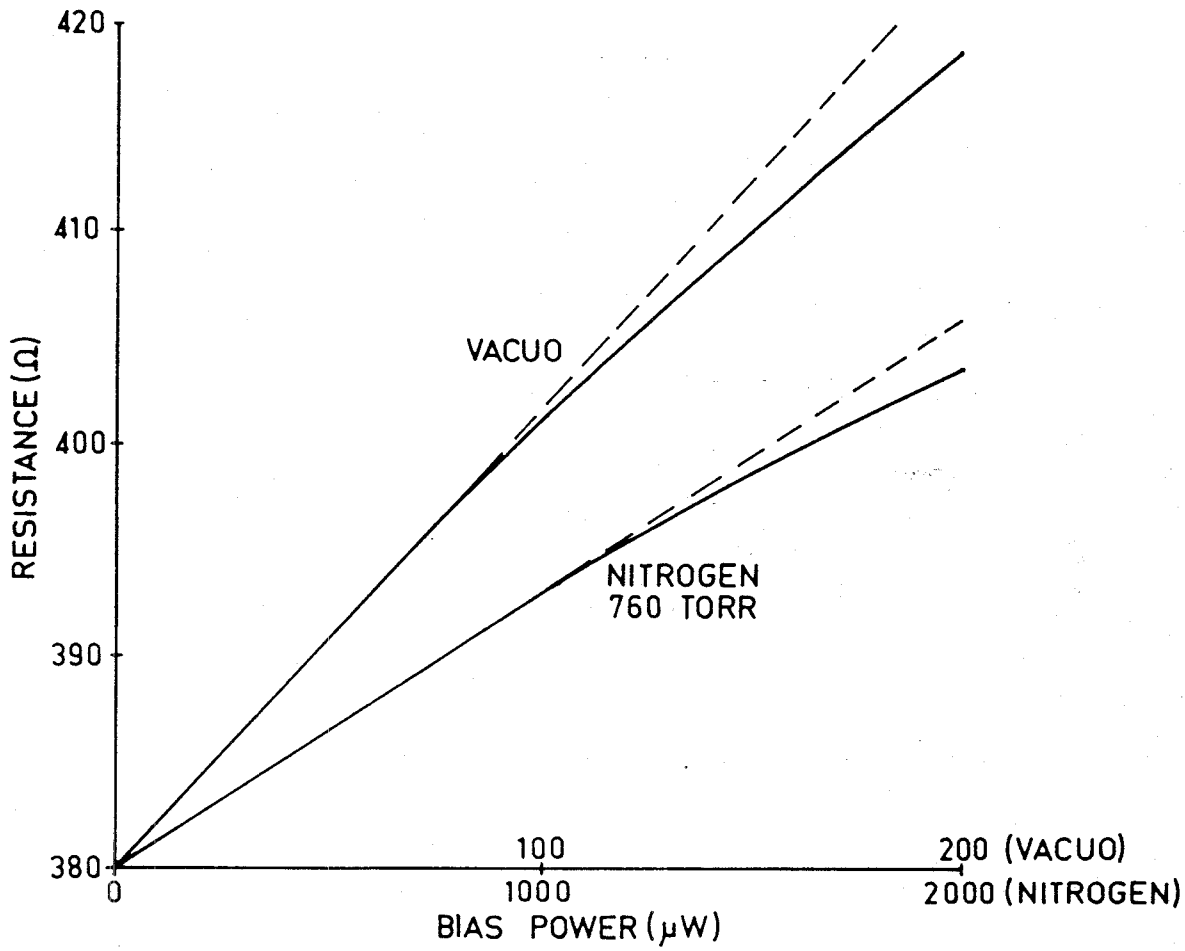

Figure 15. Plot of resistance versus bias power for a first generation detector

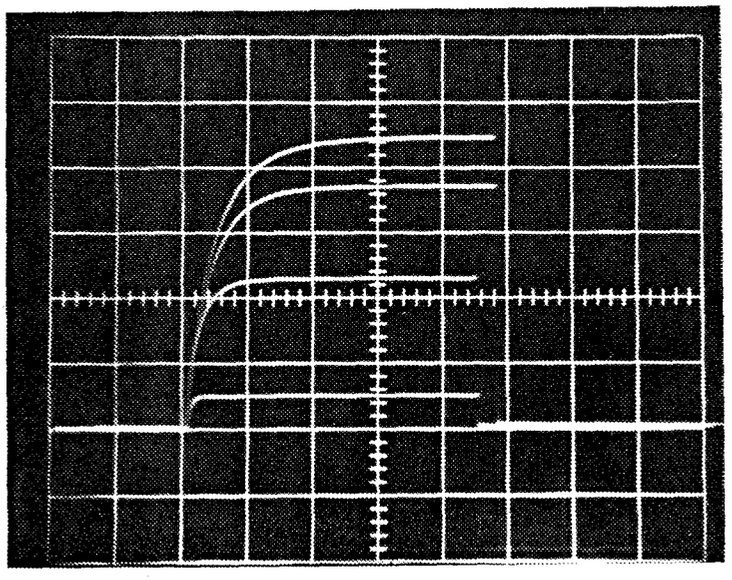

Specimen 68/2
X-axis 2 mV/div
Y-axis 2 ms/div
p=vacuo
0.1 torr
1.0 torr
10.0 torr

Figure 16. ac bias record showing detector response at different nitrogen pressures

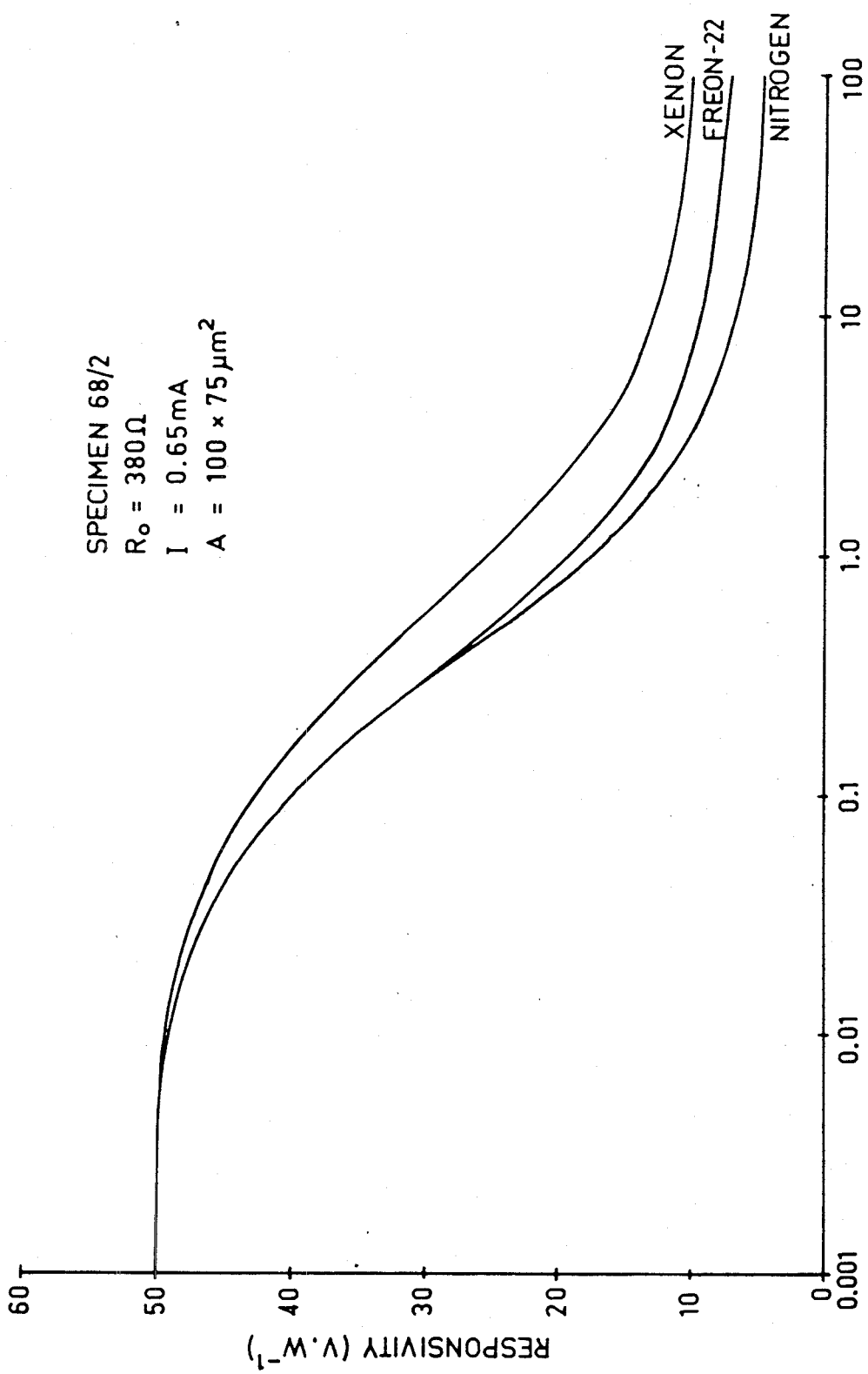

Figure 17. Low frequency responsivity as a function of gas pressure

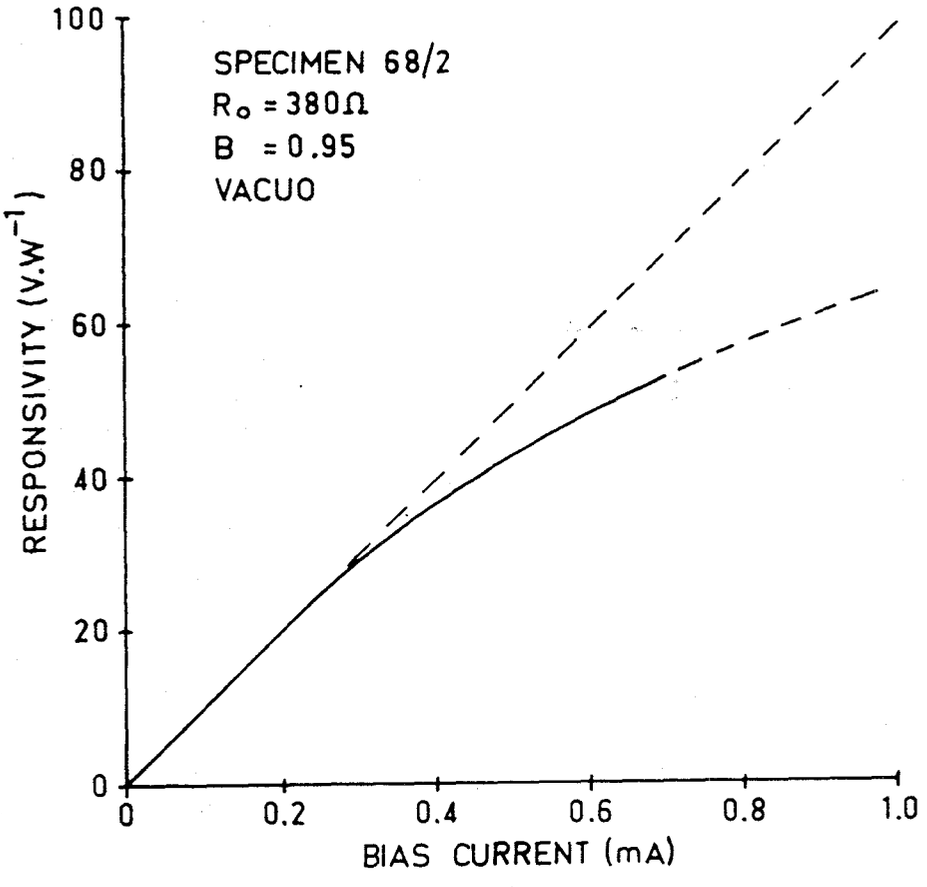

Figure 18. Vacuum responsivity as a function of bias current for a first generation detector

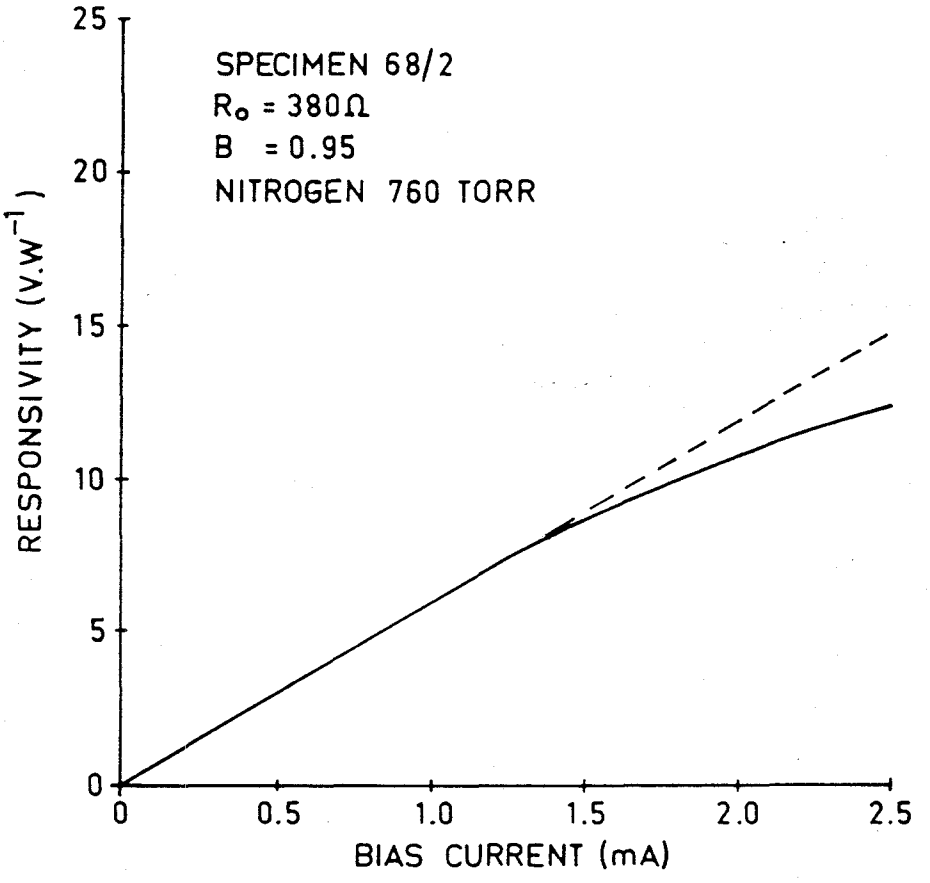

Figure 19. Responsivity at atmospheric pressure as a function of bias current for a first generation detector

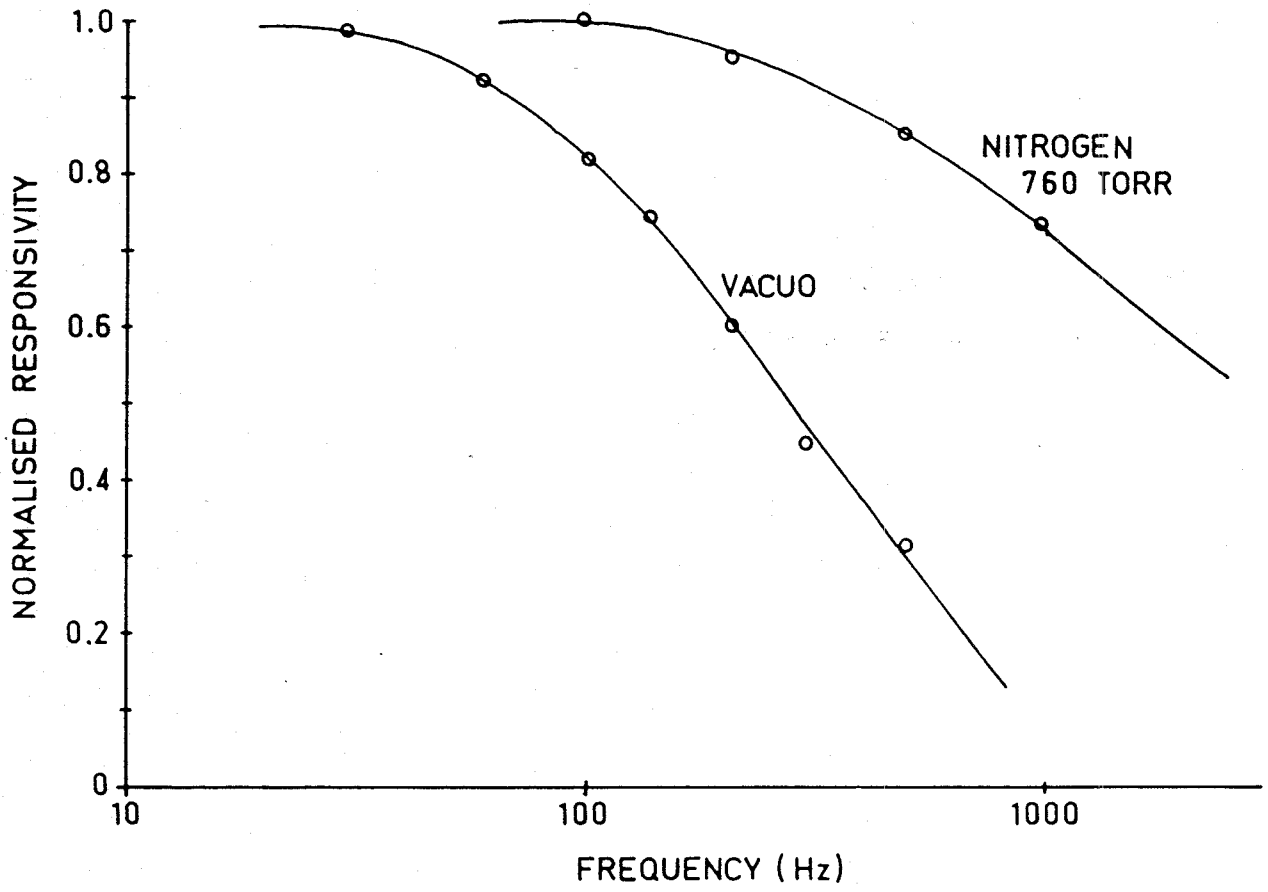

Figure 20. Frequency reponse curves for a first generation detector

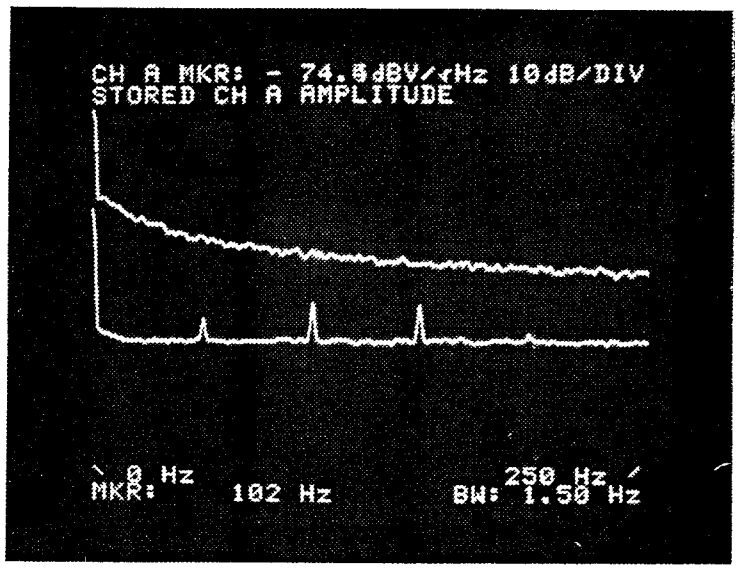

(a)

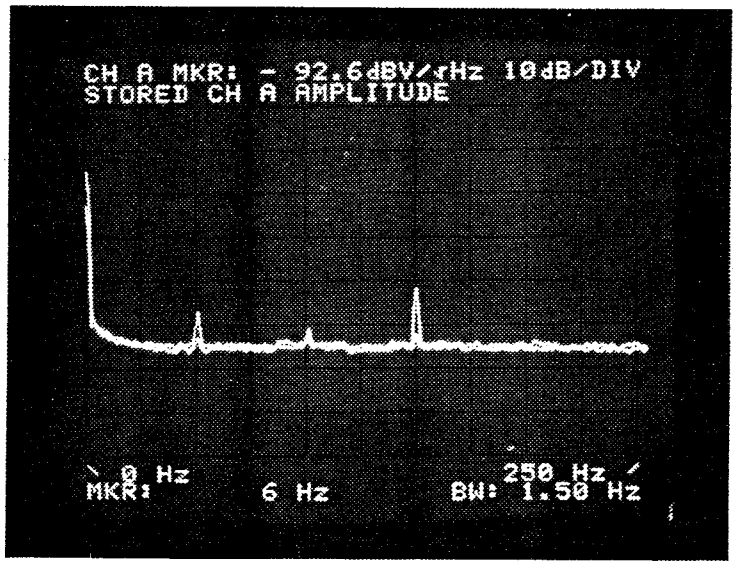

(b)

Figure 21. Spectrum analyser records of detector noise

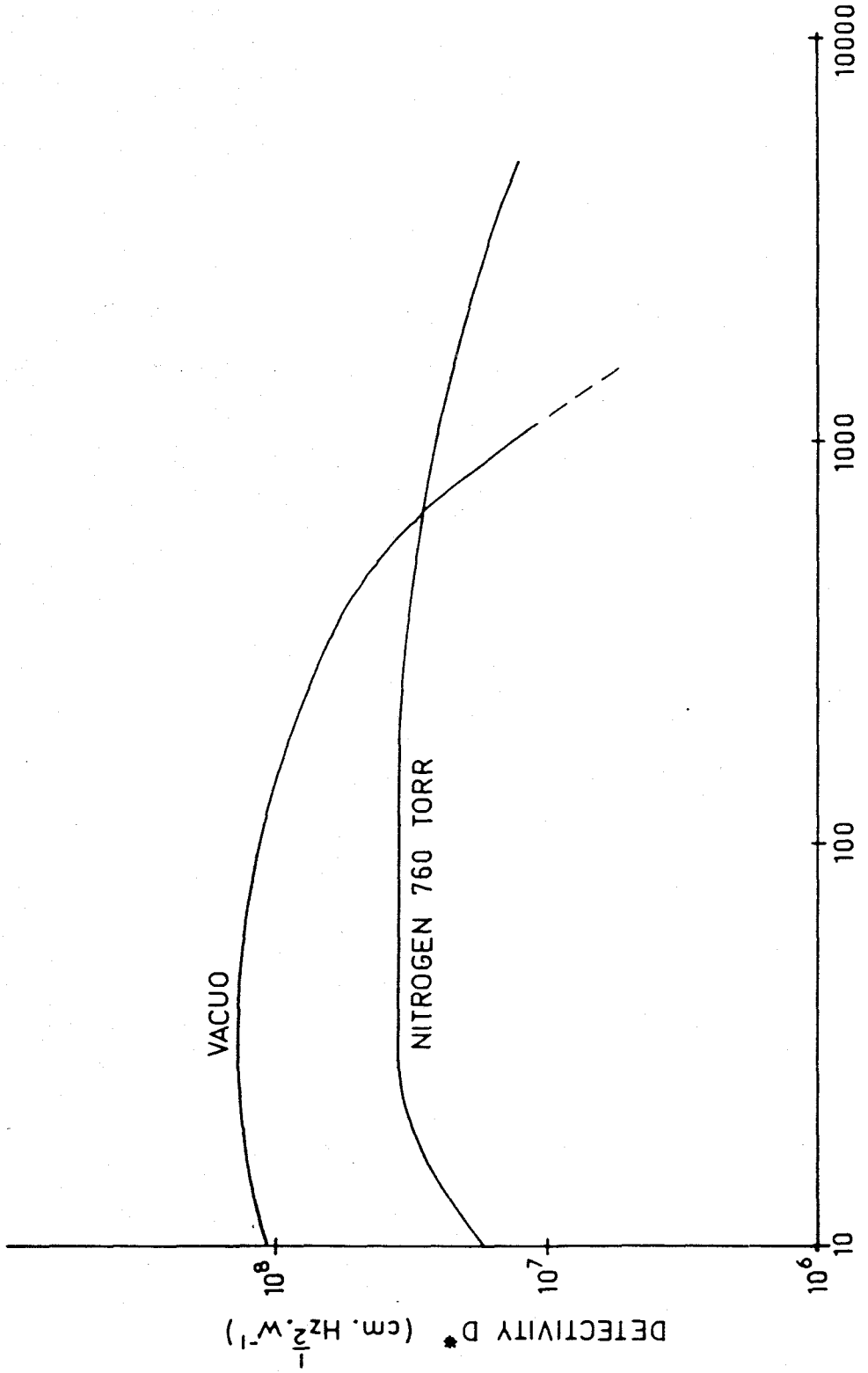

Figure 22. Detectivity as a function of frequency

DOCUMENT CONTROL DATA SHEET

Security classification of this page: UNCLASSIFIED

1 DOCUMENT NUMBERS

AR Number: AR-004-159

Series Number: ERL-0333-TR

Other Numbers:

2 SECURITY CLASSIFICATION

a. Complete Document: Unclassified

b. Title in Isolation: Unclassified

c. Summary in Isolation: Unclassified

3 TITLE

INFRARED DETECTOR RESEARCH
METAL FILM BOLOMETER DETECTORS
PART 3 - PREPARATION AND PERFORMANCE

4 PERSONAL AUTHOR(S):

K.C. Liddiard, J. Hlava and
P.D. Girdler

5 DOCUMENT DATE:

March 1985

6 6.1 TOTAL NUMBER OF PAGES 36

6.2 NUMBER OF REFERENCES: 6

7 7.1 CORPORATE AUTHOR(S):

Electronics Research Laboratory

7.2 DOCUMENT SERIES AND NUMBER

Electronics Research Laboratory
0333-TR

8 REFERENCE NUMBERS

a. Task: DST 81/146

b. Sponsoring Agency:

9 COST CODE: 635 263

10 IMPRINT (Publishing organisation)

Defence Research Centre Salisbury

11 COMPUTER PROGRAM(S) (Title(s) and language(s))

12 RELEASE LIMITATIONS (of the document):

Approved for Public Release

Security classification of this page: UNCLASSIFIED

Security classification of this page: UNCLASSIFIED

13 ANNOUNCEMENT LIMITATIONS (of the information on these pages):

No limitations

14 DESCRIPTORS:

a. EJC Thesaurus Terms

Infrared bolometers
Infrared detectors
Metal films
Detectors

b. Non-Thesaurus Terms

15 COSATI CODES:

17050

16 SUMMARY OR ABSTRACT:
(if this is security classified, the announcement of this report will be similarly classified)

This report describes the preparation and performance of metal film bolometer infrared detectors using a versatile fabrication technology for both single-element detectors and focal plane arrays. Detectors are prepared on conventional semiconductor-grade silicon substrates and extensive use is made of state-of-the-art microcircuit manufacture techniques. A detectivity of $\sim 2 \times 10^8$ cm.Hz$^{\frac{1}{2}}$.W^{-1} and speed of response of $\leqslant 1$ ms can be achieved, for detector element sizes as small as 50 μm.

Security classification of this page: UNCLASSIFIED